Taylor & Francis
Taylor & Francis Group

Journal of Building Performance Simulation

ISSN: (Print) (Online) Journal homepage: https://www.tandfonline.com/loi/tbps20

Estimating the value of jointly optimized electric power generation and end use: a study of ISO-scale load shaping applied to the residential building stock

Robert Cruickshank, Gregor Henze, Anthony Florita, Charles Corbin & Killian Stone

To cite this article: Robert Cruickshank, Gregor Henze, Anthony Florita, Charles Corbin & Killian Stone (2021): Estimating the value of jointly optimized electric power generation and end use: a study of ISO-scale load shaping applied to the residential building stock, Journal of Building Performance Simulation, DOI: 10.1080/19401493.2021.1998222

To link to this article: https://doi.org/10.1080/19401493.2021.1998222

Published online: 22 Dec 2021.

JOURNAL OF BUILDING PERFORMANCE SIMULATION
https://doi.org/10.1080/19401493.2021.1998222

Estimating the value of jointly optimized electric power generation and end use: a study of ISO-scale load shaping applied to the residential building stock

Robert Cruickshank [a], Gregor Henze [b,c], Anthony Florita [c], Charles Corbin [d] and Killian Stone [e]

[a]Consultant, Big Indian, NY, USA; [b]Department of Civil, Environmental and Architectural Engineering, University of Colorado, Boulder, CO, USA; [c]Power Systems Engineering Center, National Renewable Energy Laboratory, Golden, CO, USA; [d]Consultant, Boulder, CO, USA; [e]Consultant, Lenexa, KS, USA

ABSTRACT

A generation-to-load simulation estimated the impact, in terms of production costs and CO2 emissions, attributable to the joint optimization of electric power generation and flexible end uses to support increasing penetrations of renewable energy. Newly conceived, evaluated, and foundational in developing a U.S. National Standard was a transaction-less yet continuous demand response system based on a day-ahead optimum load shape (OLS) designed to encourage Internet-connected devices to autonomously and voluntarily explore options to favour lowest cost generators – without requiring two-way communications, personally identifiable information, or customer opt-in. Boundary conditions used for model calibration included historical weather, residential building stock construction attributes, home appliance and device empirical operating schedules, prototypical power distribution feeder models, thermal generator heat rates, startup and ramping constraints, and fuel costs. Results of an hourly-based annual case study of Texas indicate a 1/3 reduction in production costs and a 1/5 reduction in CO2 emissions are possible.

ARTICLE HISTORY
Received 26 January 2021
Accepted 18 October 2021

KEYWORDS
Co-optimization of generation and residential electric load; optimum electric load shaping; model predictive control; demand response; demand side management

1. Introduction

Geopolitical initiatives to reduce carbon emissions seek to encourage research and development of clean and inexpensive renewable energy sources (RES) (Kaufman and Gordon 2018; Bessa et al. 2019). Likewise, policies, mandates, and renewable portfolio standards attempt to drive socio-economic trends to increase the penetration of RES and raise the efficiency of existing generation (Anisie 2019). Nevertheless, nearly 3/4 of the world's electricity is still produced using steam-based thermoelectric processes that burn approximately 1/2 trillion dollars of fossil fuel per year and on average are only 1/3 efficient in converting fuel to electric power (International Energy Agency 2019; General Electric 2019).

Due to the inefficiencies of burning fuel to supply electricity, thermoelectric power plants are the largest consumers of fresh water and, along with transportation, are the largest producers of heat and greenhouse gases that trap heat (Peer and Sanders 2018; Lee et al. 2018). Thermoelectric power plants have grown in size and number over time, so much that they are among the largest contributors to anthropogenic climate change (EPA 2020). In 1882, the first coal-fired steam-powered dynamos installed in New York and London were rated to produce 100 kilowatts [kW] of power; today, more than 62,500 power plants around the world rated at 30 megawatts [MW] or greater collectively produce over 5 terawatts [TW] (Evans and Annunziata 2012).

Minimizing fossil-fuelled thermoelectric generation is not straightforward and challenges exist in maintaining the security of the electric power supply-side as providers seek the most effective mix of generators that include the highest penetration of variable-output RES (Ren21 2019; Deetjen, Rhodes, and Webber 2017). On the demand side of the electric power system, consumer privacy issues and complexities in tariff designs and regulatory structures have thwarted widespread adoption of transactive energy control and have not resulted in the load flexibility needed to support high penetrations of RES (Pratt et al. 2016).

Since its inception, electric supply has been built to anticipate and follow inflexible demand. To reverse the supply-follows-demand relationship, accelerate the penetration of RES and the beneficial electrification of transportation, buildings, industry, and agriculture – flexible demand must be encouraged to follow the cleanest and lowest cost sources of supply. Flexible demand acts as distributed storage and is fundamental and

CONTACT Robert Cruickshank rfciii@cruickshank.org Consultant, 132 Cruickshank Rd #269, Big Indian, NY 12410, USA

increasingly important in accommodating variability in RES supply while transitioning to low or zero-carbon electric power. Fortunately, the roles of flexible commercial and industrial processes in modulating demand on the grid are expanding (Eissa, Wasfy, and Sallam 2012; Ma et al. 2017). Unfortunately, though forecast with increasing accuracy (Zhang et al. 2015; Shaker, Manfre, and Zareipour 2020), residential electric loads are inflexible, operated autonomously as requested with neither regard for geographic transmission and distribution constraints nor the time-varying costs and CO_2 emissions of generating electricity.

Thermodynamics-based quantitative assessments of the generation-to-load impact of simultaneously modulating all types of flexible loads have not been widely reported. This prompted the research question: What is the overall impact of load flexibility, and in particular, how much of the overall impact can be attributed to just residential load flexibility? As such, the aim of this work was to gain an understanding of the interplay between different flexible loads and the potential size of their respective contributions in supporting society's transition to 100% RES. Perhaps flexibility having a large impact might encourage designers and regulators to further efforts in developing and legislating demand side load management. To that end, objectives included developing both a supply side model and a demand side model and then coupling and jointly optimizing them to assess the impact and value of flexibility.

This study focussed on the building-level, feeder-level, and ISO-level impact of electric loads that could be made flexible due to their inherent ability to store thermal or electrochemical energy. The analysis started at the appliance level, then aggregated load at the building, feeder, city, region, and ISO levels, while assuming continuous modulation of air conditioning, domestic hot water (DHW), and battery charging – subject to meeting occupant constraints for comfort and hot water.

To assess the maximum possible benefits of proactively shaping flexible load, the daily forecast output of all required thermal generators was flattened over time, i.e. held constant, to raise generator efficiency to minimize variable production costs. Next, the forecast time-varying generation from RES was added atop the flattened thermal generation to create an hourly day-ahead optimum load shape (OLS).

Ubiquitous internet connectivity was assumed that enabled energy retailers to broadcast the forecast OLS to automatically modulate the demand from home appliances and distributed storage to orchestrate load to flatten the output of thermal generation resources, a process that was named automatic residential load shaping (ARLS). To explore the value of ARLS end-to-end, i.e. from

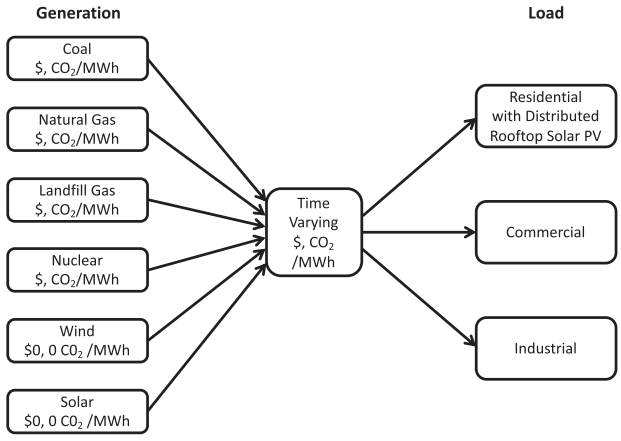

Figure 1. Variable production costs, emissions, and electricity flows.

generation to load, simulation models accounted for variable electricity production costs, CO_2emissions, flow of electricity, and load as shown in Figure 1.

Production costs of electricity varied not only with the mix of generator types and fuels, but also spatiotemporally based on local weather, which simultaneously influenced loads and, to a more significant extent, certain forms of RES generation. For example, during summer, high wind speeds from a cold front simultaneously increased the output of wind power generation and decreased the air conditioning cooling load in buildings. At times, electricity production costs were relatively low, such as when solar and wind power met most of the load. At other times, production costs were relatively high, such as when marginal power was provided by expensive peaking generators that operated for only a few hours a year, or when thermal generators operated at a partial load with relatively low heat rate energy conversion efficiencies (Mikkola and Lund 2016).

In ARLS-based joint optimization of electricity supply and demand, a benefit of flattening the load met by thermal generators was reduced startup, ramping, and shutdown of generators, which raised the overall heat rate efficiency across the entire generation fleet, thus minimizing variable production costs, particularly those related to fuel burn. Another benefit of ARLS was reducing the curtailment of RES by modulating loads to match in-time the forecast availability of wind and solar power.

The scope of this work was to quantitatively assess the overall value of completely flexible load and then estimating the subset of value attributable to just flexible residential loads. The overarching goal of this work was introducing ARLS to advance current trends to modernize generation of electricity by creating load flexibility to allow for higher RES penetration and utilization, more

efficient operation of all thermal generation, and effective transaction-less management of storage-capable distributed energy resources (DERs). The scientific contribution of this work was the creation of a method for creating, transmitting, and acting upon an OLS: (a) to evaluate the maximum value of load flexibility, and (b) to use the OLS as a control signal to manage voluntary-participating residential loads. The novelty of this work was the ability to provide novel encouraging thermodynamics-based quantitative estimates of the impact of ARLS on variable production costs and CO_2 emissions using a relatively small set of input variables.

The simulation was designed based on the following inputs: construction attributes of building stock, empirical operating schedules of all in-home end uses of electricity, prototypical electric power distribution feeder models, individual generator constraints, fuel costs, and time-synchronous historical weather, load, and RES generation data. Once calibrated using historical time-synchronous load and RES generation data, RES penetration was increased to support a sensitivity analysis of the effectiveness of ARLS in reducing both variable production costs and curtailment of RES. While required for optimizing the transmission and distribution portions of the electric grid, spatiotemporal variations in electricity cost due to grid congestion were not considered in this study. As well, control of voltage and reactive power were not considered.

The simulation environment integrated the work of Corbin and Henze (2017a, 2017b), Chassin, Fuller, and Djilali (2014), Schneider (2008), and Cruickshank et al. (2017, 2018), by taking a system-of-systems appro ach to solving the problem of jointly optimizing electricity supply and demand. Section 2 is a literature review of the value of residential electric load flexibility and models for residential electric DHW heaters and battery storage. Section 3 describes the simulation methodology. Section 4 discusses the results that motivated the development of the a U.S. National Standard for load shaping (American National Standards Institute/Society of Cable Telecommunications Engineers 2021). Section 5 presents conclusions and outlook for future work.

2. Domain-specific literature review

While reviewing the literature and available datasets for modelling grid and building interactions, several common key performance indicators (KPIs) and simulation timescales were reviewed and considered. For evaluating the potential impact of flexibility, the following KPIs were commonly used: variable electricity production costs and carbon dioxide emissions, amount of load shaped, and amount of RES curtailed. Timescales from minutes to hours were reviewed.

The simultaneous optimization of thousands of grid-interactive buildings necessitated use of a distributed optimization approach. While various modelling appro aches were considered, non-thermodynamic models such as those used in Lovins' Reinventing Fire book (Lovins 2013) were unable to perform bottom-up calculations of load and the generation required to meet load. Conversely, the thermodynamics-based HVAC component models used in many tools were suitable for performing bottom-up calculations of load, were described in detail in the EnergyPlus Engineering Reference (Energyplus 2018), and were largely derived from the American Society of Heating, Refrigerating and Air-Conditioning Engineers (ASHRAE) HVAC 2 Toolkit (Brandemuehl 1993).

OpenDSS, the Open Source Distribution System Simulator provided by the Electric Power Research Institute, has been widely used to perform grid planning studies and research (Montenegro and Dugan 2017). Since its release in 2008 as an open source platform it has become widely used. One of the features that makes OpenDSS popular is that the package offers interfaces for co-simulation, most recently with LabVIEW. Lacking was the ability to use prototypical homes to populate and model the behaviour of prototypical feeders.

GridLAB-D has also been widely used to perform grid planning studies and research, supported the ability to use prototypical homes to populate prototypical feeders, and contained a low order, four parameter thermal building model (Chassin, Fuller, and Djilali 2014; U. DOE 2017a, 2017b; Battelle Memorial Institute 2017). However, the implementation of the thermal model in GridLAB-D was not readily adaptable for distributed MPC without significant modifications to the GridLAB-D source code. Furthermore, a higher order model would likely provide greater fidelity in predicting thermal dynamics. Lacking was a tool to simulate building dynamics using a higher order model outside of GridLAB-D that was relatively simple, fast, and realistic in its predictions.

The work of Corbin and Henze (2017a, 2017b) resulted in the creation of the GridMPC (Corbin 2014) simulation environment, which was found to be suitable for building thermodynamic simulations and was shown to be successfully integrated with GridLAB-D. (Chassin, Fuller, and Djilali 2014). GridMPC struck the right balance between model complexity, accuracy, and runtime. GridMPC shaped loads based a (target) feeder reference demand signal, however, an OLS signal to drive GridMPC to minimize costs or carbon did not yet exist. GridMPC included a photovoltaic solar generation model, a physics-based building model, and the model predictive control (MPC) of residential air conditioning. Lacking

in GridMPC were models to simultaneously simulate control of air conditioning, residential electric DHW heaters and battery storage; as such, research in the below areas was reviewed to inform adding these new capabilities and degrees of control.

2.1. Value of building energy flexibility and demand response

Hungerford, Bruce, and MacGill (2019) found that de mand side management, particularly load shifting, had considerable potential to facilitate the integration of renewables. While dispatchable loads were often managed to operate off-peak late at night, they could also be managed to facilitate increasing levels of variable renewable generation. Their paper addressed the lack of data showing how dispatchable hot water systems behaved at an aggregated level in large systems using a case study of the Australian National Electricity Market (NEM). Optimized dispatch of generation within the PLEXOS® for Power Systems software environment demonstrated the potential to decrease production costs as well as reduce conventional generator cycling requirements, reduce peak demand and improve RES utilization in high renewables scenarios. Missing from the research were the impacts of simultaneously controlling water heating, air conditioning, and battery charging.

In addition to the PLEXOS production cost modelling platform, Soroudi's textbook included nearly a dozen examples for power system optimization modelling using the General Algebraic Modelling System (GAMS) (Soroudi 2017). Tips for how to start coding in GAMS were included for beginners, simple but practical examples were presented and solved, economic dispatch and several advanced topics were covered and solved. The intended audience included power system engineers, educators, system operators, and researchers, and helped users to perform modelling in GAMS as an alternative to PLEXOS or MATLAB®.

Li et al. (2016a, 2016b) focussed on the coordination of a population of thermostatically controlled loads (TCLs) with unknown parameters to achieve group objectives. The problem involved designing the device bidding and market clearing strategies to motivate self-interested users to realize efficient energy allocation subject to a peak energy constraint. The model did not include a numerical solution, renewable energy sources, distributed generation or storage, and did not specify a timescale.

Liu et al. (2014a) focussed on pricing data center demand response. The model included many system-level characteristics including collocated and offsite distributed PV generation and storage along with a numeric solution, 46, 47 and 56-bus networks, and a 5-minute timescale. Results highlighted the flexibility provided by data centers is as valuable as, and often more valuable than, the flexibility provided by large-scale storage when it comes to ensuring that a distribution network meets its voltage constraints in the presence of a large-scale solar (PV) installation. The model did not include residential buildings or loads.

Kessels et al. (2016) presented key lessons on how to encourage households to adjust energy end use by means of dynamic tariffs. The paper identified four key hypotheses related to fostering demand response through dynamic tariff schemes and examined whether these hypotheses could be accepted or rejected based on a review of published findings from a range of European pilot projects. The authors qualitatively concluded that dynamic pricing schemes have the power to adjust energy consumption behaviour within households (this is not a surprise), but did not go so far as to offer quantitative estimates.

2.2. Electric domestic hot water heaters

B. Hendron, Burch, and Journal (2010) and R. Hendron and Engebrecht (2010) provided benchmarks and illustrative methods for analyzing the energy use of modern appliances and houses. According to their research, the energy savings possible for DHW systems depends significantly on detailed occupant water use patterns. Quantifying these patterns, as surrogate measures for occupancy and energy usage, was essential for modelling water heating loads. In their work, a spreadsheet tool generated a series of year-long hot water draw schedules consistent with realistic probability distributions of start time, duration, variable flow rates, fixture types, vacation periods, and seasonality.

Burch (2012) simulated annual performance ratings for solar water heaters using weather for a typical meteorological year and then proposed a revised water draw criteria and model. Bias stemming from the lack of realism in the then-existing draw profiles included: (1) low flow rates incorrectly boosted system performance with load-side heat exchangers; (2) low mains temperature incorrectly boosted performance for all solar water heaters, and (3) an invariant draw profile could not appropriately credit larger storage volumes vs. smaller, and did not portray realistic variations in the south to north geographies. A more-realistic ratings draw was proposed that eliminated most bias by improving mains inlet temperature and by specifying more realistic hot water use. Their paper outlined the current and proposed draws and then estimated changes from draw specification changes for typical systems in four cities. The average change in the

ratings from the proposed draw was approximately eight percent.

Two-node electric resistance water heater models are often used to strike a balance between prediction accuracy and computation speed. Compared to a one-node model, the two-node model of Kondoh, Lu, and Hammerstrom (2011) captured the stratification phenomenon in the tank, thus representing the outlet temperature more accurately. Similarly, the following two-node electric domestic hot water heater model was provided in Jin et al. (2017):

$$T_{wh}^{low}(t+1) = \frac{1}{C_{wh}^{low}}[UA_{wh}^{low}(T_{air}^{in}(t) - T_{wh}^{low}(t)) + \Delta m(t)C_p(T_{inlet}(t) - T_{wh}^{low}(t)) + \eta_{wh}^{low}P_{wh}^{nom,low}U_{wh}^{low}(t)] \quad (1)$$

$$T_{wh}^{up}(t+1) = \frac{1}{C_{wh}^{up}}[UA_{wh}^{up}(T_{air}^{in}(t) - T_{wh}^{up}(t)) + \Delta m(t)C_p(T_{wh}^{1}(t) - T_{wh}^{up}(t)) + \eta_{wh}^{up}P_{wh}^{nom,up}U_{wh}^{up}(t)] \quad (2)$$

$$T_{wh}(t+1) = T_{wh}^{up}(t+1) \quad (3)$$

where superscripts *low* and *up* represented the lower node and upper node of the tank.

Equations (1) and (2) produced the water temperature as a function of the input variables. T_{wh}^{i} was the water temperature and U_{wh}^{i} was the control signal of tank node i in terms of duty cycle. T_{air}^{in} was the indoor air temperature, and T_{inlet} was the inlet water temperature. UA_i was the product of the heat loss coefficient and surface area of node i, Δm was the flow rate of hot water draws, C_p was the heat capacity of water, C_{wh}^{i} was the thermal capacitance of tank node i, and $P_{wh}^{nom,i}$ and η_{wh}^{i} were the rated power and efficiency of the resistive element in node i, respectively. Equation (3) indicated the temperature at which the hot water is delivered by the top node of the water heater. Their water heater model was subject to the following constraints:

$$T_{wh}^{min} \leq T_{wh}^{up} \leq T_{wh}^{max} \quad (4)$$

$$T_{wh}^{low} \leq T_{wh}^{up} \quad (5)$$

$$U_{wh}^{low} \leq U_{wh}^{up} \leq 1 \quad (6)$$

$$0 \leq U_{wh}^{low}, \quad U_{wh}^{up} \leq 1 \quad (7)$$

where Equation (4) dictated the temperature constraints as the hot water exits the tank from the upper node. Equation (5) enforced the thermal stability in the tank such that the lower node should not be hotter than the upper node because of buoyancy. Equations (6) and (7) were the constraints of control signals U_{wh}^{low} and U_{wh}^{up} which were continuous variables between 0 and 1 that could be interpreted as duty cycles.

Though heat pump water heaters provide savings in heating hot water and are increasing in popularity, they were not included in the literature review or analysis. That said, heat pump water heaters would likely have (a) less instantaneous load shed capability due to reduced load from a compressor being used most often for heating versus a heating element, and (b) similar load add capabilities when energizing a heating element.

The literature reflects a general agreement on (a) the importance of DHW draw schedules as a proxy for energy use, and (b) the use of two-node models to capture the operating characteristics of DHW heaters.

2.3. Distributed battery storage of electrical energy

Barley et al. (1995) and Barley and Winn (1996) defined energy storage cost and explored dispatch optimization strategies to minimize costs associated with generator starts, generator fuel consumption, and battery erosion, based on an economic analysis of present worth life-cycle cost. They documented the case when the load is large enough – and thus the generator fuel efficiency is high enough – that the cost of diesel generation per unit of energy produced is less than the cost of battery wear; they defined a critical load, L_d, above which this applies and developed a 'frugal discharge strategy'.

More recently, Kaabeche and Ibtiouen (2014) developed metrics for comparing and sizing hybrid photovoltaic, wind, diesel, and battery generation in a standalone power system. A techno-economic approach combined two models: A reliability model developed based on the total energy deficit concept and an economic model based on the calculation of total net present cost. The combination determined the optimum configuration in the most cost-effective manner. Optimization results showed that a combined photovoltaic, wind, diesel, and battery system was more economically viable compared to either (a) a photovoltaic, wind, and battery system, or (b) a diesel generator only.

In a grid-tied battery system with dynamic pricing (Newsham and Bowker 2010), Newsham et al. found the added dimensions of buying and selling electricity at different prices at different times of the day helped make a case for local micro-controllers and new battery storage operating paradigms as implemented by Sklar (1990).

Liu et al. (2014b) studied pricing-based demand response and concluded that large loads could provide nearly the same degree of flexibility for load-serving entities as does large-scale storage – if adequately incentivized. However, and this was a significant caveat, there was more planning of lead-time required (i.e. it was more

compute intensive) to extract flexibility from loads than from (battery) storage.

Per Jin et al. (2017), battery state of charge (SOC), charging power, P_{bat}^{ch}, and discharging power, P_{bat}^{dis}, were related as follows:

$$SOC(t+1) = SOC(t) + \frac{\eta_{bat}^{ch}\Delta t}{Q_{bat}} P_{bat}^{ch}(t) + \frac{\Delta t}{\eta_{bat}^{dis} Q_{bat}} P_{bat}^{dis}(t) \tag{8}$$

where $P_{bat}^{ch} \geq 0$, $P_{bat}^{dis} \leq 0$, and η_{bat}^{cha} were the discharging and charging efficiency of the battery system, $\Delta(t)$ was the length of the prediction step, and Q_{bat} was the capacity of the battery. The battery control variables were $U_{bat}^{ch} = P_{bat}^{ch}/P_{batt}^{ch,max}$ and $U_{bat}^{dis} = P_{bat}^{dis}/P_{batt}^{dis,max}$ which represented the percentage of maximum charging power, $P_{bat}^{ch,max}$, and maximum discharging power, $P_{bat}^{dis,max}$, respectively.

The battery system model in Equation (8) was subject to the following constraints:

$$SOC^{min} \leq SOC(t+1) \leq SOC^{max} \tag{9}$$

$$0 \leq U_{bat}^{ch}(t), \quad U_{bat}^{dis}(t) \leq 1 \tag{10}$$

where Equation (9) defined the operable SOC range for reducing battery degradation and Equation (10) indicated the range of the normalized battery control variables.

In addition to thermal energy storage in buildings and appliances, electrical energy storage in distributed fixed and mobile batteries has proliferated and introduced additional degrees of freedom for control for home energy management systems (Jin et al. 2017). Batteries are unique in their ability to provide a near-instantaneous response in load add and shed – and can be very flexible over short time frames (I. Tesla 2019). In conjunction with one-time optimum sizing of a battery system and related charging and discharging components, several factors that govern efficient charging and discharging of batteries must be continuously considered in order to provide optimum supervisory control.

The literature suggests that there are likely significant economic opportunities enabled by battery storage. This is especially true given recent trends away from net-metering (where buying and selling costs are equal per unit of electricity e.g. per kWh) toward feed-in tariffs, where selling cost is a fraction of buying cost. Lower feed-in tariffs give rise to the need for optimum control that can manage the 'buying low and selling high' of electricity and promote self-consumption on-site.

3. Simulation methodology

In order to leverage available data sources (Craig et al. 2019; National Oceanic and Atmospheric Administration 2019) and appropriately answer research questions, a 1-hour simulation time step for generation and a 5-minute time step for building thermodynamic response and load were chosen for simulating the impact of ARLS. The simulation incorporated functionality for the model predictive control of buildings developed by Corbin and Henze (2017a, 2017b), the modelling of electrical distribution feeders developed by Chassin, Fuller, and Djilali (2014), Schneider (2008), and an electricity production cost model (PCM) developed within the General Algebraic Modelling System (GAMS) using GAMS Studio version 0.14.3 and solved using IBM C-PLEX version 12 (Soroudi 2017). In the spirit of transaction-less yet continuous distributed control, the simulation intentionally spanned across markets and assumed the remuneration for consumers would be accomplished using existing interval metering and billing infrastructures along with electricity pricing based on time-of-use or dynamic tariffs.

For load modelling, GridMPC was chosen for its ability to include device-level and building-level responses in distribution grid simulations, utilities for parsing simulation input files and weather files, writing files required by the power flow simulation software, and its building model that improved fidelity, e.g. beyond GridLAB-D (Chassin, Fuller, and Djilali 2014) with reasonable simulation run times. The building thermal model in Corbin and Henze (2017a, 2017b) and Cruickshank et al. (2018), as incorporated into GridMPC (Corbin 2014), was suitable for use without modification. However, extensions to GridMPC were required to provide for additional degrees of control in order to simultaneously optimize electrical energy use by DHW heaters and battery systems. The GridMPC DHW heater model was replaced to allow for simulating: (a) dynamic thermal behaviour, (b) MPC-enabled setpoint changes, and (c) usage schedules that reflected empirical behaviour (Cruickshank et al. 2017), e.g. as observed in the Northwest Energy Efficiency Alliance, Residential Building Stock Analysis: Metering Study (Larson et al. 2014). The solar penetration assumptions from GridMPC were adjusted to reflect 50% and 100% of homes having annual net-zero solar generation. A new model was developed for the MPC of battery charging and discharging. For modelling production cost, GAMS was chosen as it has been shown to produce results comparable to a commercial tool such as PLEXOS® (Helistö et al. 2019), is widely available, provides for the use of many different solvers including the IBM C-PLEX solver used in many operations research practices, and is highly configurable in the creation and solution of

energy systems models. A random generator uncertainty model was developed to evaluate the impact of planned and unplanned generator outages on production costs and CO_2 emissions.

To set up a simulation, (1) Buildings were chosen from the Energy Information Agency, Residential Energy Consumption Survey (RECS) database (U.S. Energy Information Administration 2009), and (2) local weather was used by GridMPC to auto-size the annual required air conditioning capacity and the required area for a net-zero solar array. To run a simulation, the following steps were followed:

(1) For each of 365 days, use hourly weather to calculate load and distributed solar generation for each building.
(2) Sum building loads across feeders.
(3) Scale feeders to regional loads and then sum across regions.
(4) Remove utility-scale wind and solar generation.
(5) Run GAMS production cost model to calculate lowest ops cost and resulting CO_2 emissions for *unshaped* thermal generation.
(6) Calculate daily forecast Optimum Load Shape.
(7) Re-run production cost model to calculate lowest operating cost for *optimally shaped* (flattened) thermal generation.
(8) Compare costs and CO_2 emissions for unshaped versus optimally shaped load.

3.1. Mathematical formulation and simulation model

The mathematical formulation of the Unit Commitment model constructed in GAMS consisted of a cost-optimization objective function based on production costs:

$$\min\left\{\sum_{t=1}^{n}\left\{\sum_{i=1}^{N} v_i c_i(p_i)\right\}\right\}, v_i \in \{0,1\} \qquad (11)$$

which was constrained by the need to match supply and demand in each time period:

$$\sum_{i=1}^{N} p_i = d \qquad (12)$$

where:

n was the number of time intervals in each optimization step
N was the total number of generators
v_i was the binary variable indicating whether a generator is committed (1) or not (0)
c_i was the operating cost of generator i ($US/MW)
p_i was the power generation of generator i (MW)
d was the system demand (MW)

Simulations were performed three times to estimate the impacts in costs and CO_2 emissions attributable to jointly optimizing electric power generation and use via ARLS. In each simulation, a primary GAMS-based PCM simulated the costs and emissions of the thermal generators that met the net load (i.e. the total load less RES generation), and a secondary GAMS model determined the daily optimum 'flat' net generation shape. Then, RES was added to the daily optimum net generation shape to produce the daily OLS. Considered case studies included the model predictive control (MPC) of various storage-capable end uses and scenarios included increasing penetration of RES.

First, *actual* production costs, emissions, and OLS were estimated based on actual historical load. Second, *simulated* production costs, emissions and OLS were estimated based on a simulated historical load obtained by coupling local historical weather and residential building stock data with the calibrated residential building model (Corbin and Henze 2017a, 2017b). Third, costs and CO_2 emissions were estimated based on the *simulated* MPC of the on/off setpoints of end-use loads in various RES scenarios. A high-level representation of the ARLS simulation is shown in Figure 2.

Starting at the left of Figure 2, regional parameters were selected for building stock. Next, auto-sizing of system nominal capacities based on annual local weather was performed for air conditioning, DHW, and solar PV systems. Load simulation was performed per feeder, aggregated to cities, and scaled to weather zones. Daily variable production costs and OLS were calculated and broadcast to MPC-enabled controllers in each home, which, with knowledge of forecast weather, occupant comfort constraints, and home/away schedules, autonomously explored ways to shape loads to minimize deviations from the OLS.

In each simulation, a PCM-based economic unit commitment of all required generators minimized the variable production cost per day by choosing the lowest cost mix of generators for every hour, subject to operating characteristics and constraints including: Base heat rate [MMBTU]: the fuel burned to keep a generator at operating temperature; marginal heat rate [MMBTU/MWh]: the fuel burned by a generator to produce electrical output; maximum generator capacity [MW]: the maximum output of a generator; minimum generator capacity [MW]: the minimum output of a generator; maximum upward and downward ramping [MW/hour]: the maximum increase and decrease in the output of a

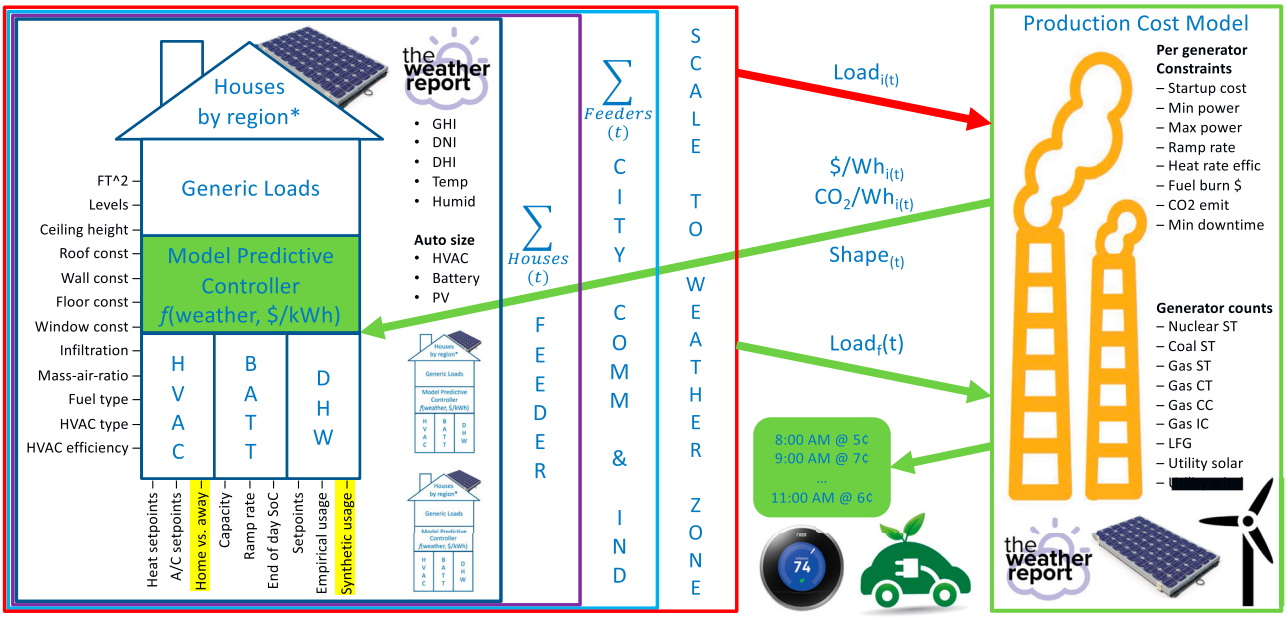

Figure 2. Automatic Residential Load Shaping simulation. $Load_{i(t)}$ denotes initial load. $Load_{f(t)}$ denotes optimized load. Weather parameters include global horizontal irradiance (GHI), diffuse horizontal irradiance (DHI), direct normal irradiance (DNI). Generator types include steam turbines (ST), combustion turbines (CT), combined cycle (CC), internal combustion (IC) and landfill gas (LFG). The OLS is denoted by $Shape_{(t)}$. Variable production costs and CO_2 emissions as a function of time are also shown.

generator in a single hour (note that thermal generators ramp slowly in comparison to gas turbines); variable operation and maintenance cost, VO&M [$/MWh] per generator, which increased with output power; startup cost [$/start]: related to the type of fuel and time required to start a generator, typically from a cold-start condition; fuel price [$/MMBTU] for different fuel types; minimum down time constraint (hours), the amount of time required to take a generator offline and then bring it back online again; and CO2 emission rate [lb/MMBTU]: the emissions per unit of fuel consumed by a generator.

3.2. Electric domestic hot water heater loads

An evaluation was performed on the electric hot water heater physical model in GridLAB-D (Battelle Memorial Institute 2017) and found it lacking in realism. As a result, an 'instantaneous' two-node physical model was created. The model ran on a one-second timescale and was originally written in Python. The model was ported from Python to Java so that it could be incorporated into GridMPC. The Java version was verified against the original Python version by setting the same initial conditions (tank geometry, volume, and insulation characteristics) and runtime conditions (inlet water temperature, thermostat setpoint and dead band, and water draws) and then verifying the energy consumption and water outlet temperature over time. The ported instantaneous Java model was then extended for simulation timescales of several minutes. After satisfactory testing, the model was incorporated into GridMPC. In attempting to follow the daily OLS, MPC adjusted the water temperature setpoints causing an electric water heater to store and release thermal energy over time.

3.3. Distributed battery storage of electrical energy

The battery model was designed from first principals, following the method (Jin et al. 2017), and could be thought of as a hydraulic reservoir where water height represented the state-of-charge (SOC). In general, house loads discharged the battery and charging offset loads; this is where the height of reservoir analogy applied, e.g. if the load (out) was greater than charge (in), then the battery discharged (i.e. the water level dropped).

At each timestep, the GridMPC particle swarm optimizer (PSO) adjusted the power supply control vector, which contained setpoints for the upper value of SOC and a global lower bound. Battery discharge was equal to the sum of all house loads, including air conditioning, DHW heating, and appliances. Multiple runs were completed with various PSO simulation settings to verify the desired operation in finding a global rather than local minimum.

The battery was modelled with no standby losses (i.e. it maintained its charge over time). SOC was constrained to equal 50% at the beginning and end of every daily simulation which: (a) ensured that batteries were ready to charge or discharge at the start of simulation, and

(b) simplified checksum calculations for the conservation of energy. The battery model assumed a combined 89% round trip charge and discharge efficiency (calculated during charge) (I. Tesla 2019), no standby losses, and a maximum hourly charging rate of 25% of battery size. The battery was sized at 13.5 kWh, as commonly found in a Tesla Powerwall (I. Tesla 2019). In attempting to follow the daily OLS, MPC adjusted the SOC setpoints causing batteries to charge and discharge over time.

3.4. Battery key performance indicators

Metrics used to capture battery performance and the cost of control included: (a) *AV*, the sum over the simulation of the absolute value of changes in the state of charge, *SOC*, e.g. $AV = abs(+5\%) + abs(-2\%) = 7\%$ over two intervals, and (b) *Ls*, the percent of load shaped. The *AV* battery metric was designed to measure how 'hard' a battery worked and aggregated the total amount of energy passing through a battery over time expressed as a percent of battery capacity. Note that *AV* could rapidly exceed 100%, which was expected behaviour and was important in forecasting battery life-cycle cost due to wear and tear from charging and discharging. *Ls* was defined as the sum over the simulation intervals of the absolute values of the deltas between the shaped and unshaped load and had units of energy. As a percentage, *Ls* became a normalized value when divided by the sum of energy delivered in the unshaped case.

3.5. Distributed generation via residential solar photovoltaic collectors

Solar array sizing for each house was based on net-zero energy consumption on an annual basis. To create three scenarios of increasing RES penetration, each of 14 unique feeders with 0% distributed solar photovoltaic (PV) penetration was replicated once to include 50% of houses having PV and then again to include 100% of houses having PV. In the 50% percent penetration case, every other house on a feeder was chosen to have PV. The houses with and without PV were kept as a static set when performing subsequent simulations.

3.6. Summary of simulation and model validations

The thermodynamic building model was validated on an annual basis using BESTEST-EX (Corbin 2014). The testing procedure included a suite of building physics test cases used to validate GridMPC's ability to correctly capture building cooling load calculations on an annual basis for a variety of different building configurations in various climates; a sub-hourly validation was also performed at a 5-minute time step. Appliance and DHW heater load models were validated based on observed empirical loads in the RBSA study (N. RBSA 2017). The generator and production cost models were validated based on the NREL production cost study that used the same generators and unshaped load (Craig et al. 2019). The battery model was validated using a first law of thermodynamics checksum that included charging losses.

3.7. Texas case study

A case study simulated electricity generation and use across the serving area of the Electric Reliability Council of Texas (ERCOT). Texas was chosen to study for several reasons:

(1) It has over 24 million electricity customers across residential, commercial, and industrial sectors.
(2) It uses approximately 1 TWh of electricity on an average day and is responsible for roughly 10% of U.S. and 2% of world energy use (Electric Reliability Council of Texas 2019a).
(3) It has distinct climate regions across 200,000 square miles.
(4) Its historical weather, time-synchronous load and RES data are available for different weather load zones.
(5) It can be modelled as an electrical island due to its limited imports and exports of electricity.
(6) Its generation mix includes many RES and fossil-based technologies and more than 600 fossil-based generators of various sizes and constraints (Craig et al. 2019).

Figure 3 depicts three Texas climate regions (3, 4, and 5) as defined by the Pacific Northwest National Laboratory (PNNL) (Schneider 2008) and eight coloured weather load zones (Electric Reliability Council of Texas 2019b) as defined by ERCOT.

The case study consisted of (1) unshaped and optimally shaped cases for actual and simulated ERCOT load, (2) seven combinations of the model predictive control (MPC) of residential air conditioners, electric DHW heaters, and battery charging systems, and (3) three scenarios of increasing RES penetration. In addition, the case study included the operating characteristics, constraints, and fuel costs of 263 utility-scale thermal generators that closely represent ERCOT generation (Craig et al. 2019). An excerpt of the ERCOT generation fleet is listed in Table 1. Note that generators were, for the most part, individual line items, though in some cases were grouped as a single meta generator, e.g. in the last two rows of Table 1,

Figure 3. ERCOT operating area with three PNNL Grid Taxonomy climate regions separated by dashed lines and eight coloured weather zones (adapted from Electric Reliability Council of Texas 2019b and Schneider 2008).

utility-scale wind and solar generators were grouped by technology.

To assess variability in production costs due to scheduled and unscheduled maintenance of generators, a sensitivity analysis was used to estimate variable production costs and emissions based on the random unavailability of generators (NRDC 2020). For a given daily net load, the PCM used a random sample of available generators. A Monte Carlo method repeatedly chose a random set of available generators to arrive at the expected mean production cost and a distribution thereof.

3.7.1. Estimated production cost and emissions based on actual electricity use

For Case 1, Actual Load, production costs and emissions were estimated for the ERCOT-recorded 2005 hourly load less the time-synchronous electricity production of all utility-scale wind and solar generators (Electric Reliability Council of Texas 2005). Time-synchronous load and renewable generation data for more recent years was unavailable. The hourly GAMS PCM used inputs of net load, generator characteristics and constraints. The time-varying blended costs, marginal costs, and CO_2 emissions were simulated based on the constraint of thermal generation equaling net load for each hour. In keeping with best practices for PCM validation, the simulated variable production costs were compared to the actual production costs for the same period to check for general agreement (Craig et al. 2019). Representing approximately 1%

Table 1. Sample ERCOT generator characteristics and constraints.

Unit	County	Fuel	Prime Mover	Capacity (MW)	Marginal HR (MMBtu/MWh)	BaseHeat Rate (MMBTU)	Co2Ems (lb/MMBtu)	VOM ($/MWh)	MinLoad (MW)	StartCost ($)	MinDownTime (hrs)	RampRate (MW/hr)	FuelPrice ($/MMBtu)
BRAUNIG_AVR1_CT1	bexar	GAS	CC	533.0	9.3	154.5	117.0	3.7	213.2	49690.0	4	169.5	3.3
ATKINS_ATKINSG7	brazos	GAS	GT	18.0	12.8	0.0	117.0	15.7	7.2	419.5	1	6.2	3.3
DG_WALZE_4UNITS	bexar	LFG	LFG	9.8	13.8	0.0	117.0	8.9	3.9	456.8	4	3.4	0.0
CALHOUN_UNIT1	calhoun	GAS	ST	44.0	12.3	102.7	117.0	4.5	17.6	4102.0	7	10.2	3.3
COLETO_COLETOG1	goliad	COAL	ST	655.0	10.4	1284.1	214.3	4.5	327.5	61063.7	12	117.2	2.2
CPSES_UNIT1	somervell	NUCLEAR	ST	1205.0	10.5	0.0	0.0	2.2	1084.5	561693.2	20	96.4	0.7
WT-ercot1	kinney	WIND	WT	20200.8	0.1	0.0	0.0	0.0	0.0	0.0	0	20200.8	0.0
PV-ercot1	presidio	SOLAR	PV	1003.8	0.0	0.0	0.0	0.0	0.0	0.0	0	1003.8	0.0

Note: Prime movers include Gas Combined Cycle plants (CC), Gas Turbines (GT), Landfill Gas plants (LFG), Gas and Coal Steam Turbines, Wind Turbines (WT) and Photovoltaic (PV) generators. Not shown but included are: Internal Combustion (IC) and Combustion Turbine (CT) prime movers.

of generation, 745 MW of Texas utility-scale hydroelectric power was excluded to simplify the analysis.

For Case 2, Daily OLS, to support the calculation of the minimum possible variable production cost, a simplifying assumption was made that all load could be shaped with negligible losses and penalties. While unrealistic due to the efficiency and standby losses of electrical and thermal storage, the negligible losses assumption enabled the daily-based GAMS PCM to enforce a constraint of thermal generation equaling net load for an entire day as opposed to thermal generation equaling net load for every single hour of a day. In the *daily-based* PCM, the simplifying assumption always resulted in a constant output thermal generation shape with no generator starts, stops, or ramping. The flat thermal generation shape resulted in the lowest variable production cost and as such was considered the daily optimum, albeit highly idealized,s thermal generation shape. As a last step in Case 2, the *hourly-based* PCM used a flat daily optimum net generation shape to calculate the hourly production costs and emissions.

3.7.2. Estimated production cost and emissions based on simulated ERCOT electricity use

For Case 3, Simulated Base Case load, the thermodynamic model of residential buildings (Corbin and Henze 2017a, 2017b), provided a five-minute time-series estimate for each of the 8 ERCOT weather zones and for ERCOT in total. Individual cities in each of the eight ERCOT weather zones referenced the local airport time-synchronous weather denoted by the short form of the International Civil Aviation Organization airport identifier (e.g. Houston denoted by HOU) (International Civil Aviation Organization 2019). For weather details, see the 2005 annual files of hourly observations across Texas (National Oceanic and Atmospheric Administration 2019). Per the PNNL grid taxonomy, between four and eight of the 14 feeders unique to ERCOT appeared in each city resulting in a total of 48 'city' feeders as shown in Table 2, where the letter R denotes residential feeders and the letters GC denote generalized commercial feeders.

GridLAB-D MATLAB scripts provided by PNNL (Pacific Northwest National Laboratory 2018) populated the simulation files for each unique feeder by selecting house attributes from the RECS database (U.S. Energy Information Administration 2009). GridMPC then used the reduced-order thermal building model and historical weather to simulate hourly thermal and electrical load in homes; it simplified each home in GridLAB-D into an equivalent ZIP load model so that the homes within the feeder could be simulated simply as an electric demand calculated outside of GridLAB-D. This was accomplished by first writing the electric demand of each home at each time step of the simulation into a separate file, then linking these files to the power flow simulation using the GridLAB-D ZIPload and player objects. The new model that resulted, which combined the loads calculated by GridMPC with the GridLAB-D feeder model, was termed the 'hybrid model' and produced GridLAB-D output files for each feeder (Corbin 2014).

Table 2. ERCOT PNNL feeders by Weather Zone, city, and airport.

Weather Zone	City	Airport Weather	Feeders
West	Abilene	ABI	4
	R4-12.47-1/2, R4-25.00-1, GC-12.47-1		
N. Central	Dallas	RBD	4
	R4-12.47-1/2, R4-25.00-1, GC-12.47-1		
Coast	Houston	HOU	8
	R5-12.47-1/2/3/4/5, R5-25.00-1, R5-35.00-1,GC-12.47-1		
Southern	Laredo	LRD	8
	R5-12.47-1/2/3/4/5, R5-25.00-1, R5-35.00-1, GC-12.47-1		
North	Lubbock	LBB	4
	R3-12.47-1/2/3, GC-12.47-1		
Far West	Midland	MAF	4
	R3-12.47-1/2/3, GC-12.47-1		
South	San Antonio	SAT	8
	R5-12.47-1/2/3/4/5, R5-25.00-1, R5-35.00-1, GC-12.47-1		
East	Tyler	TYR	8
	R5-12.47-1/2/3/4/5, R5-25.00-1, R5-35.00-1, GC-12.47-1		

Simulations of each of the feeders, including a complete set of miscellaneous loads and appliances were performed per house and then summed to produce the aggregate loads per feeder without MPC control. This was referred to as the Base Case simulation and included all residential loads from electrically powered devices such as water heaters, refrigerators, ranges, computers, televisions, cable boxes, and lighting. Referencing the percent proportion of each feeder type within a region described by Schneider (2008), the feeder loads were summed proportionally to simulate the per day five-minute city loads.

To scale-up city loads and create aggregate weather zone loads, the daily sum of the historical actual hourly weather zone load was divided by the daily sum of simulated city load in order to arrive at a city-to-zone scaling factor. City-to-zone scaling factors were calculated for all eight weather zones and used as multipliers of five-minute city loads in order to arrive at aggregate calibrated five-minute weather zone loads. The sum of loads used in the calibration produced a zero bias (i.e. there was no residual in the annual energy balance); alternatively, calibration via nonlinear minimization could be used to minimize the variance between the actual and simulated loads using a Newton-type algorithm with a non-zero bias. Lastly, the aggregate five-minute load per weather zone was summed across all weather zones to create an unshaped Base Case (BC) aggregate five-minute ERCOT load.

As a final step in Case 3, the *hourly-based* PCM returned the variable production costs and emissions for meeting the aggregated (unshaped) load across ERCOT. Case 4, Simulated Base Case OLS, followed the same procedure as Case 2, in this case, applied to the simulated load of Case 3. Cases 5–8 are the daily excerpts from Cases 1–4, respectively.

3.7.3. Estimated production cost and emissions based on simulated MPC-based load shaping

For Cases 9 through 15 of simulated shaped loads, ARLS extended the MPC-based load shaping and air conditioning models of Corbin and Henze to include control of electrical charging of batteries and thermal charging of electric DHW heaters. Using ARLS, a set of cases and scenarios assessed the cost and CO_2 impact of different combinations of controlled end uses, e.g. air conditioning only, air conditioning plus battery charging, air conditioning plus battery charging plus electric water heating.

A set of cases implemented the following steps: (1) MPC shaped electric load by optimizing the above end-uses based on forecast weather, predetermined presence of occupants assumed to be away from home from 8 AM to 6 PM, bounded temperature setpoints, and target load shape deltas derived from the daily OLS, (2) Loads were aggregated across Texas using feeder-to-weather zone scaling, and the residential load was estimated to be 33% of total load with the remaining load assigned to commercial and industrial loads, (3) For the three scenarios of RES penetration (A) low, (B) medium, and (C) high, the variable production costs and CO_2 emissions from generators operating to meet the MPC-managed load were summarized.

3.7.4. MPC scenarios

The MPC of air conditioning systems followed the method of Corbin and Henze to auto-size the cooling capacity for each home based on the maximum cooling day for the year and a ten-minute minimum on-time for single-stage air conditioning. In attempting to follow the daily OLS, MPC adjusted the cooling setpoints causing houses to store and release thermal energy over time.

In Cases 9–15, MPC attempted to meet the daily OLS, and the resulting shaped load was input to the hourly PCM, which returned costs and emissions for each ERCOT simulation scenario. To accommodate the additional degrees of MPC control, particle swarm parameters were adjusted based on results of experiments to determine the appropriate parameters. The MPC control intervals were increased from 30-minutes to 1-hour to limit oscillatory behaviour of loads and to reduce computer processing time.

3.7.5. PSO optimization parameters

The GridMPC air conditioning model used an increment of 0.25 K and a maximum particle velocity of 0.25 K. To reflect allowable temperature ranges during home and away occupant hours, GridMPC was allowed to explore a range of thermostat settings including 2 K below the setpoint while the occupants were home, and from 5 K below to 3 K above the setpoint while the occupants were away.

Extending the work of Corbin and Henze (2017a, 2017b), the PSO parameters were set such that there were 24 dimensions, 1 per hour, for every controlled device, resulting in a total of 72 dimensions for the case of air conditioning plus battery plus water heater (AC+BAT+WH). The control resolution was set to 0.25 K for air conditioning and DHW heater models and to 1% of capacity for the battery model. The maximum particle velocities were chosen by graphing the swarm behaviour for individual houses, manually inspecting graphs of multiple runs, and then choosing velocities which showed asymptotic convergence within 5000 iterations. The maximum velocities for the AC, battery, and water heater were 0.25, 2, and 24, respectively.

The water heater model operated over a temperature range of −10 to +10 K. Given an increment of 0.25 K, the max velocity of the particles was four increments, equal to 4/80 or 5% of the total search space for each dimension. The battery model had a charge range of −50% to +50% from an initial 50% SOC, with each value representing one percentage point of battery capacity. Given the increment of 1%, the maximum velocities of the particles was 24 increments equal to 24/100 of the total search space for the first 20 dimensions (i.e. the first 20 hours of the day). Dimensions 20–24 had their lower and upper bounds decreased by 12.5% each so that all batteries would attempt to converge to 50% charge by the end of the day.

4. Results

In simulations of generation and load across ERCOT, cost and CO_2 emission estimates for actual, simulated, and MPC-managed loads quantified the impact of optimum load shaping for various penetrations of utility wind, utility solar and distributed solar photovoltaic generation. Using inputs of the forecast load, generation from RES, thermal generator properties, and fuel costs, the hourly PCM produced a daily unit-commitment of the generation mix to estimate lowest possible electricity production cost. Using the daily OLS as an input control signal, MPC enabled the optimal supervisory control of the thermal and electrical energy storage in each house. Comparing the daily electric power production costs and

Table 3. Full year 2005 range of variable production costs and CO_2 emissions for actual load, simulated load, and scenarios of increasing RES penetration.

Scenarios ⟶		A. Low RES penetration uWind22, uSolar1, dSolar0			B. Medium RES penetration uWind30, uSolar3, dSolar50			C. High RES penetration uWind38, uSolar5, dSolar100		
↓ Cases		Cost	Cost	CO_2	Cost	Cost	CO_2	Cost	Cost	CO_2
Full year 2005		$ [B]	$/MWh	lb [B]	$ [B]	$/MWh	lb [B]	$ [B]	$/MWh	lb [B]
1	Actual load observed in Texas	5.36	17.96	252	3.75	12.58	146	3.22	10.77	94.7
2	…daily optimum shape	5.31	17.80	257	3.23	10.83	148	1.92	6.44	77.9
3	Simulated Base Case load	5.35	17.92	253	3.49	11.70	138	2.92	9.79	84.0
4	…daily optimum shape	5.30	17.76	263	3.14	10.53	141	1.70	5.70	65.0

Notes to Table 3: (1) Curtailment of uWind and uSolar was required during some hours in Scenario B and many more hours in Scenario C in order to prevent over generation.(2) Uncertainty in production cost due to random generator unavailability due to planned and unplanned maintenance was less than x%.Entries for utility-scale wind and solar denote penetration based on annual production, e.g. uWind22 denotes utility wind providing 22% of the annual energy in 2005. Entries for distributed solar, e.g. dSolar50, denote the percent of houses with PV.

resulting emissions over a number and type of distributed storage degrees of freedom controlled by MPC, resulted in a range of costs and CO_2 emissions.

4.1. Cost and emissions overview

Table 3 is a summary of ERCOT annual production costs and CO_2 emissions. Each row depicts a different case of actual and simulated load; each column depicts three scenarios of (A) low, (B) medium, and (C) high penetrations of RES. In each group, the daily optimal load shape was applied to the actual and simulated load to flatten net generation and determine the lowest possible production cost. The difference in production cost to serve the load with and without the optimal load shape determined the upper bounds of possible reductions in variable costs and CO_2 emissions.

Table 3, Scenario A, Cases 1 and 3 reflect good agreement between the annual cost of providing electricity Texas-wide, which was approximately $5.3B in 2005. Results from all scenarios indicated a reduction in costs in Cases 2 and 4 when the OLS was applied. Scenario A savings were 1%, Scenario B savings were approximately 10%, and Scenario C savings were approximately 40%. Savings in Scenarios B and C are attributable to ARLS shaping and modulating load to better match in time the available RES, which resulted in decreased curtailment of RES and lower costs.

With respect to CO_2 emissions, Cases 2 and 4 have a 2% to 3% increase from Scenario A to Scenario B; in large part due to increased use of lower cost but higher CO_2-producing coal steam turbines which displaced the use of cleaner gas combined cycle generation. Most notably, Scenario C provided an approximate 20% decrease in CO_2 attributable to ARLS' reduced curtailment use of RES.

Table 4 summarizes the 1-day results for Cases 5–15 for 18 May 2005, which is illustrative of Spring and Fall weather. RES penetration Scenarios A, B and C are the same is in Table 3. Cases 5, 6, 7, and 8 are 1-day excerpts of Cases 1, 2, 3, and 4 in Table 3. Cases 9 through 15 quantify the performance of the MPC of air-conditioning, battery charging, and electric DHW heating.

In Table 4 Scenario A, Cases 5 and 7 have reasonable agreement between the daily cost of providing electricity Texas-wide, which was approximately $13M for the day. The most substantial decreases in production cost occurred across all scenarios in Cases 6 and 8 when OLS was applied. As summarized with relative percentages in Table 5, Case 8, Scenario A had a 5% decrease in cost, Scenario B had a 65% decrease in cost, and Scenario C had no impact as RES and nuclear generation met the load for all Cases. Cases 9–15, Scenario A had a range of cost impacts from −3% to +10%. Cost increases were due to overall increased energy use in optimization cases due to standby losses associated with pre-cooling a home and pre-heating hot water. Cases 9–15, Scenario B had 1% to 19% reductions in cost, with lowest cost in Case 10.

With respect to CO_2 emissions, in Table 5, Case 8, Scenario A had a 22% increase, Scenario B had an 86% decrease, and Scenario C had no impact as RES and nuclear generation met the load for all Cases. As will be shown in Section 4.2, increases in emissions are due to the decreased use of cleaner but more expensive and more flexible gas generation, and increased use of dirtier, but less expensive and less flexible coal generation. Cases 9–15, Scenario A had a 4% to 11% increase in emissions. Scenario B indicates an 2% to 22% decrease in emissions, with the lowest emissions in cases 13 and 15.

Table 6 summarizes the single-day results for Cases 5–15 for 23 August 2005, which is illustrative of a Summer peak demand day. RES penetration Scenarios A, B and C are the same is in Tables 3 and 4. As in Table 4, Cases 5, 6, 7, and 8 are single-day excerpts of Table 3 and Cases 9 through 15 quantify the performance of MPC.

In Table 6, Case 5, Scenario A, the daily production cost of $25.4M is significantly less than the Case 7 cost of $31.5M. For Scenario B, there is better agreement, and Scenario C has the best agreement. The most significant reductions in cost occurred across all Scenarios in Cases

Table 4. 18 May 2005 range of variable production costs and CO_2 emissions for actual load, simulated load, and scenarios of increasing RES penetration.

Scenarios ⟶		A. Low RES penetration uWind22, uSolar1, dSolar0			B. Medium RES penetration uWind30, uSolar3, dSolar50			C. High RES penetration uWind38, uSolar5, dSolar100		
↓ Cases		Cost	Cost	CO_2	Cost	Cost	CO_2	Cost	Cost	CO_2
18 May 2005		$ [M]	$/MWh	lb [M]	$ [M]	$/MWh	lb [M]	$ [M]	$/MWh	lb [M]
5	Actual load observed in Texas	12.96	15.45	486	6.73	8.02	160	3.67	4.37	52.00
6	…daily optimum shape	11.25	13.41	523	3.63	4.32	119	1.07	1.28	8.00
7	Simulated Base Case load	12.10	14.43	447	3.07	3.66	59	1.07	1.28	8
8	…daily optimum shape	11.44	13.64	547	1.07	1.28	8	1.07	1.28	8
9	Simulated load with MPC A/C	12.39	14.77	484	2.79	3.33	53	1.07	1.28	8
10	…with MPC BAT	11.78	14.04	476	2.5	2.98	46	1.07	1.28	8
11	…with MPC DHW	12.24	14.59	466	3.03	3.61	53	1.07	1.28	8
12	…with MPC A/C + BAT	13.29	15.84	489	2.56	3.05	48	1.07	1.28	8
13	…with MPC A/C + DHW	12.52	14.92	496	2.85	3.39	58	1.07	1.28	8
14	…with MPC BAT + DHW	11.96	14.25	484	2.56	3.05	53	1.07	1.28	8
15	…with MPC A/C + BAT + DHW	12.25	14.6	493	2.66	3.17	58	1.07	1.28	8

Notes to Table 4: (1) For cases 5–15, residential PV solar sizing was initially based on net zero whole-house energy usage on an annual basis and then on daily basis to reduce compute times. (2) Curtailment of uWind and uSolar is required during some hours in Scenario B and many more hours in Scenario C in order to prevent over generation.

Table 5. 18 May 2005 impact compared to unshaped actual load.

Scenarios →		Cost Impact [%]			CO2 Impact [%]		
↓ Cases		A	B	C	A	B	C
8	Simulated BC load optimum shape	−5%	−65%	0%	22%	−86%	0%
9	Simulated load with MPC A/C	2%	−9%	0%	8%	−10%	0%
10	…with MPC BAT	−3%	−19%	0%	6%	−22%	0%
11	…with MPC DHW	1%	−1%	0%	4%	−10%	0%
12	…with MPC A/C + BAT	10%	−17%	0%	9%	−19%	0%
13	…with MPC A/C + DHW	3%	−7%	0%	11%	−2%	0%
14	…with MPC BAT + DHW	−1%	−17%	0%	8%	−10%	0%
15	…with MPC A/C + BAT + DHW	1%	−13%	0%	10%	−2%	0%

6 and 8 when the OLS was applied. As summarized with relative percentages in Table 7, Case 8, Scenario A had a 3% decrease in cost, Scenario B had a 1% decrease in cost, and Scenario C had an 11% decrease in cost. Cases 9–15, Scenario A have minor cost increases, due to the standby losses related to optimization that allowed more overall – yet lower cost – energy to be used, e.g. preheating water resulted in standby losses as a tank cooled down. Cases 9–15, Scenario B had minor cost differences. Cases 9–15, Scenario C had between 0% to 9% decrease in cost.

With respect to CO_2 emissions, Case 8 had minor cost differences in Scenarios A and B and a 28% increase in Scenario C. Cases 9–15, Scenario A had minor increases from increased energy use due to the standby losses related

Table 6. 23 August 2005 range of variable production costs and CO_2 emissions for scenarios of increasing RES penetration and increasing MPC of end uses.

Scenarios ⟶		A. Low RES penetration uWind22, uSolar1, dSolar0			B. Medium RES penetration uWind30, uSolar3, dSolar50			C. High RES penetration uWind38, uSolar5, dSolar100		
↓ Cases		Cost	Cost	CO_2	Cost	Cost	CO_2	Cost	Cost	CO_2
23 August 2005		$ [M]	$/MWh	lb [M]	$ [M]	$/MWh	lb [M]	$ [M]	$/MWh	lb [M]
5	Actual load observed in Texas	25.41	22.51	1157	17.91	15.86	838	15.13	13.4	471
6	…daily optimum shape	24.31	21.54	1132	17.72	15.7	897	11.35	10.06	531
7	Simulated Base Case load	31.54	27.95	1407	20.83	18.45	948	13.34	11.82	453
8	…daily optimum shape	30.61	27.12	1412	20.66	18.31	932	11.83	10.48	579
9	Simulated load with MPC A/C	32.15	28.48	1433	21.08	18.67	959	12.93	11.45	471
10	…with MPC BAT	31.52	27.92	1406	20.61	18.26	930	12.12	10.74	474
11	…with MPC DHW	31.84	28.21	1420	20.89	18.51	953	13.35	11.83	457
12	…with MPC A/C + BAT	31.85	28.21	1422	20.97	18.58	943	12.23	10.83	483
13	…with MPC A/C + DHW	32.48	28.78	1444	21.18	18.76	947	13.10	11.61	480
14	…with MPC BAT + DHW	31.95	28.3	1408	20.74	18.38	935	12.11	10.73	484
15	…with MPC A/C + BAT + DHW	32.26	28.58	1438	21.16	18.75	952	12.44	11.02	491

Notes to Table 6: (1) For cases 5–15, residential PV solar sizing was initially based on net zero whole-house energy usage on an annual basis and then on daily basis to reduce compute times.(2) Curtailment of uWind and uSolar is required during some hours in Scenario B and many more hours in Scenario C in order to prevent over generation.

Table 7. 23 August 2005 impact compared to unshaped actual load.

Scenarios →		Cost Impact [%]			CO2 Impact [%]		
↓ Cases		A	B	C	A	B	C
8	Simulated BC load optimum shape	−3%	−1%	−11%	0%	−2%	28%
9	Simulated load with MPC A/C	2%	1%	−3%	2%	1%	4%
10	…with MPC BAT	0%	−1%	−9%	0%	−2%	5%
11	…with MPC DHW	1%	0%	0%	1%	1%	1%
12	…with MPC A/C + BAT	1%	1%	−8%	1%	−1%	7%
13	…with MPC A/C + DHW	3%	2%	−2%	3%	0%	6%
14	…with MPC BAT + DHW	1%	0%	−9%	0%	−1%	7%
15	…with MPC A/C + BAT + DHW	2%	2%	−7%	2%	0%	8%

to cost optimization. Cases 9–15, Scenario B had minor decreases. Cases 9–15, Scenario C had increases between 1% to 7% due to increased energy use and increased use of less expensive coal generation that displaced the use of more expensive cleaner gas combined cycle generation, similar to as shown in Figure 8.

In summary, the benefits in load reduction were not apparent in Scenarios A and B for at least the following reasons: (1) There was increased energy use due to the standby losses associated with shaping load, and (2) The model underpredicted high load periods, which resulted in less use of the most expensive marginal generation.

4.2. Variability in production costs due to random unavailability of generators

The variability in production costs and CO_2 emissions due to scheduled and unscheduled maintenance and outages of individual generators is shown in Figure 4, which depicts results of a cost-based sensitivity analysis using a random sample of available generators meeting the load over 24 hours on 1 January 2005. Results are shown for 100%, 97.5%, 95%, 92.5%, and 90% of the ERCOT of fleet generators being available. Lower numbers of available generators results in only slightly higher costs due to relatively small differences in the marginal costs of available versus unavailable generators. However, lower numbers of available generators results a greater impact on raising emissions due to the larger differences in the emissions of available versus unavailable generators, e.g. the emissions from an available coal generator are greater than those of an unavailable gas generator.

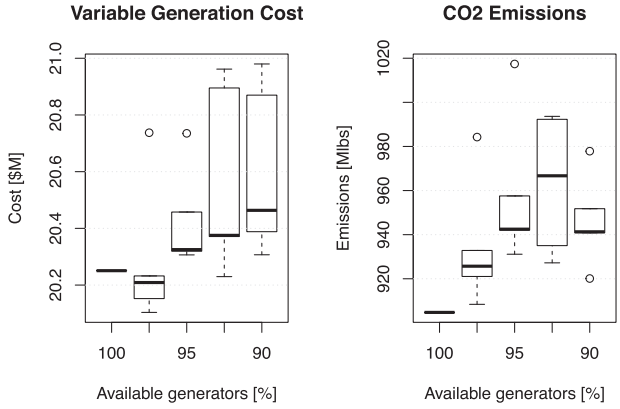

Figure 4. Variability in production costs and CO_2 emissions due to random unavailability of generators on 1 Jan 2005.

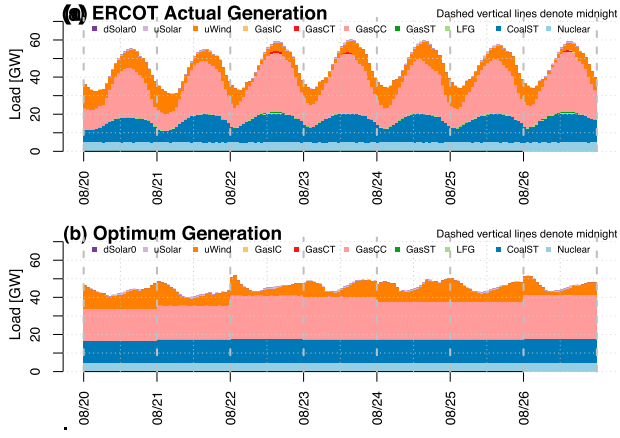

Figure 5. ERCOT hourly generation based on actual load at top (a) and daily optimum load at bottom (b) on 20–26 Aug 2005.

4.3. Unshaped actual load versus optimum load shape

For Cases 1 & 2, Scenario A, production cost and CO_2 emissions were calculated for the unshaped *actual* historical hourly load and for the same load had it been optimally shaped over seven days as shown in Figure 5(a,b), respectively. As expected, the minimum production cost was achieved when the net load was constant, depicted as flat lines for thermal generation, as shown for each hour of 20–26 Aug 2005 in Figure 5(b). The week of 20–26 August is of interest as: (a) it was the hottest week of 2005 with over a TWh of energy delivered each day, and (b) many of the 263 thermal generators were active and could benefit from higher capacity factors.

Figure 5 is known as a generation stack and depicts the cumulative contributions of 10 power production generation technologies that together meet the time-varying load. In Figure 5(a) there are a peak hours of dark red

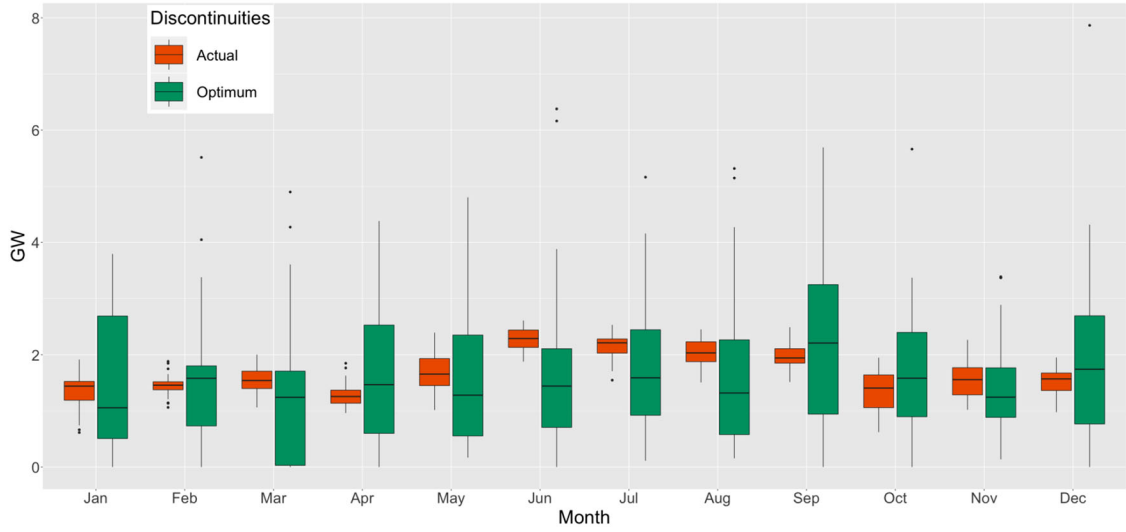

Figure 6. Box plot distributions of daily midnight generation discontinuities for 2005.

(GasCT) in-between the bands of orange (uWind) and light red (GasCC) on 22, 23, and 26 August, and there are peak hours of dark green (GasST) above the dark blue (CoalsST) on 22 and 26 August. Barely visible are small diurnal midday generation contributions in light purple (uSolar) at the very top of each graph, and a very thin continuous thread of light green (LFG) atop the dark blue (CoalST) generation.

In Figure 5(a), note the net generation ramped up and down (depicted by seven humps) in shades of blue and red as the ERCOT generation fleet varied its production of electricity to meet the net demand. As expected, for a daily optimum shape, the ramping of thermal generation in (a) is removed, as shown by flat net generation in (b) where there is no intra-day ramping in the dark blue (CoalST) and light red (GasCC) generation. The result is an impact on variable production cost and CO_2 emissions of individual generators. Summing across all generators and time, the total energy delivered in (a) and (b) is the same except for standby losses, i.e. the areas under and including the topmost curves in (a) and (b) are nearly the same.

As depicted in Figure 5(b), the daily optimum shape can result in step change discontinuities on day boundaries at midnight, e.g. between midnight on 22 August and 1 AM on 23 August. Discontinuities were the result of adjacent days with different aggregate energy use and, as expected, were minimal between days with similar energy use and meteorological conditions. Typical discontinuities in load, defined as those observed in Case 1 (historical data), were compared to the discontinuities in Case 2 (OLS). Box plot distributions of discontinuities in Cases 1 and 2 provide a sense of typical vs. atypical behaviour, as shown per month in Figure 6.

In Figure 6, the monthly median of midnight discontinuities is less for the optimum versus the actual load in January, March, May through August, and November. Small midnight discontinuities are advantageous from the perspective of reduced thermal and pressure stresses that result from ramping thermal generators (Miller et al. 2014). Nonetheless, the upper quartiles and inter-quartile ranges in all months depict many greater than typical midnight discontinuities. Methods for reducing midnight discontinuities are likely to include modifications to the GAMS PCM to manage day-to-day boundaries and are beyond the scope of this research.

Hourly outputs from the Texas fleet of RES and non-RES generators were compared and contrasted for Scenarios A, B, and C. Sample visualizations of the generation that met the load for each hour of 23 August 2005 are shown in Figures 7, 8, and 9. In each figure, Cases and Scenarios are denoted with an abbreviated notation, e.g. C5SA denotes Case 5, Scenario A. In Figure 7(a,b), the visualizations are a single-day zoomed view of the 23 August 2005 weekly view in Figure 5.

Figure 7(a) depicts the variability in unshaped load and generation in 24 hourly intervals. The variability in utility wind power (uWind 22) is denoted by the changing height of the orange bars, with output lowest from sunrise through hour 11. To ramp up output and meet the daily peak load, GasCT generation was required for hours 14, 15, and 16.

The top line in Figure 7(b) provides visual insight to creating the daily OLS. In the first of two steps, the thermal generation in Figure 7(a) was flattened, i.e. held constant, by equally distributing the sum of daily non-RES production across all 24 hours, in this example starting with the light blue (Nuclear) fleet at the bottom up to and

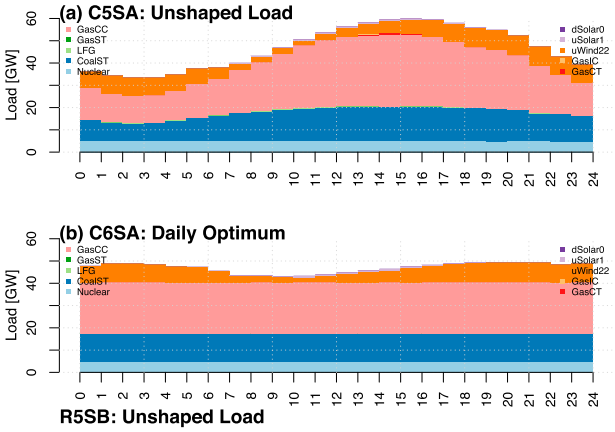

Figure 7. Cases 5 & 6, Scenario A, ERCOT generation that met the actual unshaped load at the top (a) and optimal generation at the bottom (b) for 23 Aug 2005. Between (a) and (b), the percent of load shaped, *Ls*, is 21%.

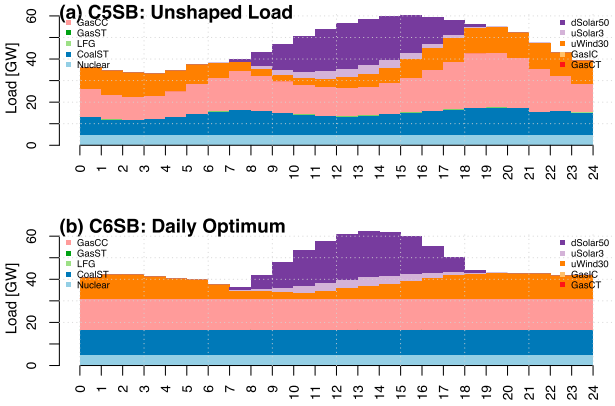

Figure 8. Cases 5 & 6, Scenario B, ERCOT generation that met the actual unshaped load at the top (a) and optimal generation at the bottom (b) for 23 Aug 2005. Between (a) and (b), the percent of load shaped, *Ls*, is 29%.

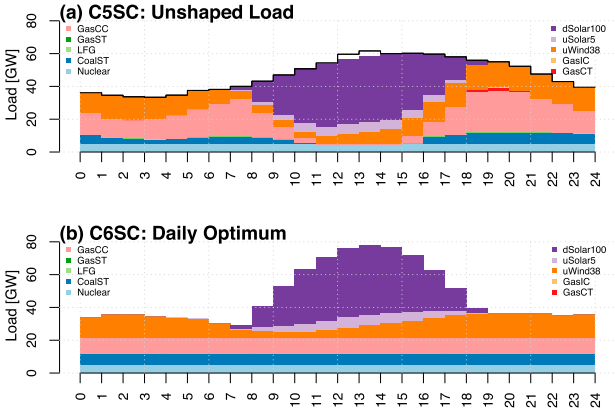

Figure 9. Cases 5 & 6, Scenario C, ERCOT generation that met the actual unshaped load at the top (a) and optimal generation at the bottom (b) for 23 Aug 2005. Note the black trace at top in (a) denotes curtailed RES which is zero at bottom in (b). Between (a) and (b), the percent of load shaped, *Ls*, is 59%.

including the light red (GasCC) fleet. In the second step, the hourly variable RES generation was added atop the flattened thermal generation, in this case resulting in a somewhat concave optimal load shape.

As shown in the legend of Figure 8, Scenario B introduced: (a) increased utility wind (uWind) from 22% to 30% of the total annual ERCOT production, (b) increased utility solar (uSolar) from 1% to 3% of the total annual ERCOT production, and (c) distributed net-zero solar PV on 50% of homes.

For the Unshaped Load, increasing RES increased the ramping of thermal generation as can be observed by comparing Figures 7(a) and 8(a). Figure 8(a) shows more up and down ramping of net generation to accommodate the increase in variable RES. For the Daily Optimum, the impact on the thermal generation fleet of increasing RES can be observed by comparing and contrasting Figures 7(b), and 8(b). In addition, the impact of increasing RES on the peak output of thermal generation can be observed by comparing Figure 7(b), where the top of the thermal generation is a flat line at 40 GW, and Figure 8(b), where the top of the thermal generation is reduced to 30 GW, representing a one-quarter reduction between Scenarios A and B.

As shown in Figure 9, Scenario C further increased: (a) uWind to 38% of the total annual ERCOT production, (b) uSolar to 5% of the total annual ERCOT production, (c) dSolar to 100% of homes.

For the Unshaped Load, further increasing RES had an additional impact on thermal generation that can be seen by comparing Figures 7(a), 8(a), and 9(a). Figure 9(a) shows a further increase in the ramping of net generation to accommodate the increase in RES. During daylight hours, the increased contributions of distributed solar generation required: (a) downward ramping through noon to prevent over-generation, and then (b) upward ramping through hour 19 to ensure supply would meet demand. Approaching noon, downward ramping required the GasCC and CoalST fleets to completely shut down by hour 11. During hours 12 and 13 the top black line depicts renewable energy overgeneration that had to be curtailed (i.e. could not be used and was thrown away). The four nuclear power plants in light blue remained operational per the constraint that they could not shut down for short intervals. During the afternoon, the CoalST and GasCC generation fleet ramped up, and at hour 18 and 19 upward ramping was supplemented by the fast-starting and fast-ramping GasCT fleet.

For the Daily Optimum, comparing and contrasting Figures 7(b), 8(b), and 9(b) provides insights to the impact on the thermal generation fleet of further increasing RES. In Figure 9(b) the top of the non-RES generation fleet

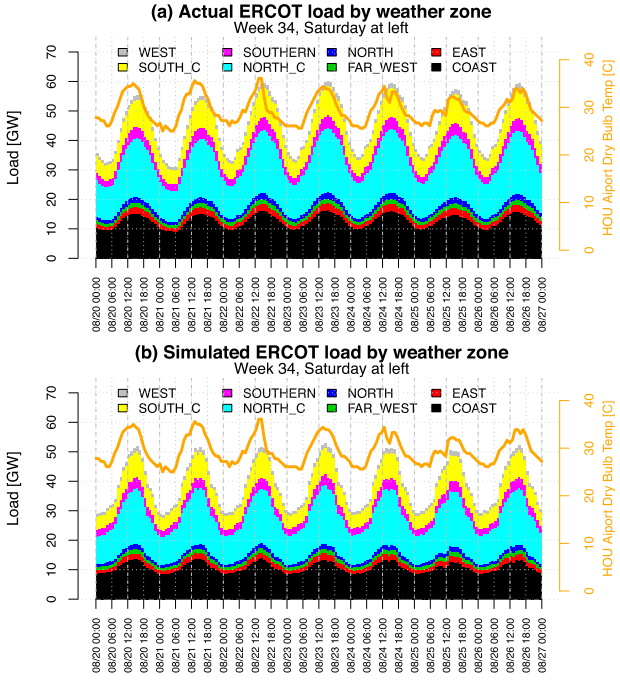

Figure 10. ERCOT load per weather zone. Actual at top and simulated at the bottom on 20–26 August 2005. For reference, Houston airport temperatures are shown at far right. The two highest demand weather zones are home to Houston in the Coast region (in black at the bottom) and Dallas in North Central (in light blue in the middle).

is a flat line reduced to just over 20 GW, representing a nearly one-half reduction in thermal generation between Scenarios A and C.

4.4. Simulated load

Historical electricity use was simulated using the building model with local weather inputs, aggregated by feeder, scaled from feeder to city, and then city to weather zone. The actual and simulated load by weather zone is shown in Figure 10 using a different scheme of eight colours representing the ERCOT weather zones. The two largest weather zones are the Coast (in black), in which Houston is located, and North Central (in light blue), in which Dallas is located. Summing the historical observed load per weather zone provided a total ERCOT load which peaked near 60 GW during the middle of the week.

As expected, the impact of outdoor temperature on load was found to be significant. For reference, in Figure 10, Houston temperatures are shown as a gold line with a scale on the right vertical axis. The position of the gold temperature line is unchanged in (a) and (b). Referencing the gray topmost load curve against the gold temperature line provides insight to the magnitude of the errors between the (a) actual load, and (b) simulated load. The errors are a result of the model underpredicting simulated load.

To investigate model prediction errors, frequency distributions (histograms) were created to provide insight to the skill of the model throughout the forecasting regime. The 2005 actual and simulated total and net loads are depicted in Figure 11.

In Figure 11(a), note the long tails in the actual load in the upper row that are missing in the (b) bottom row

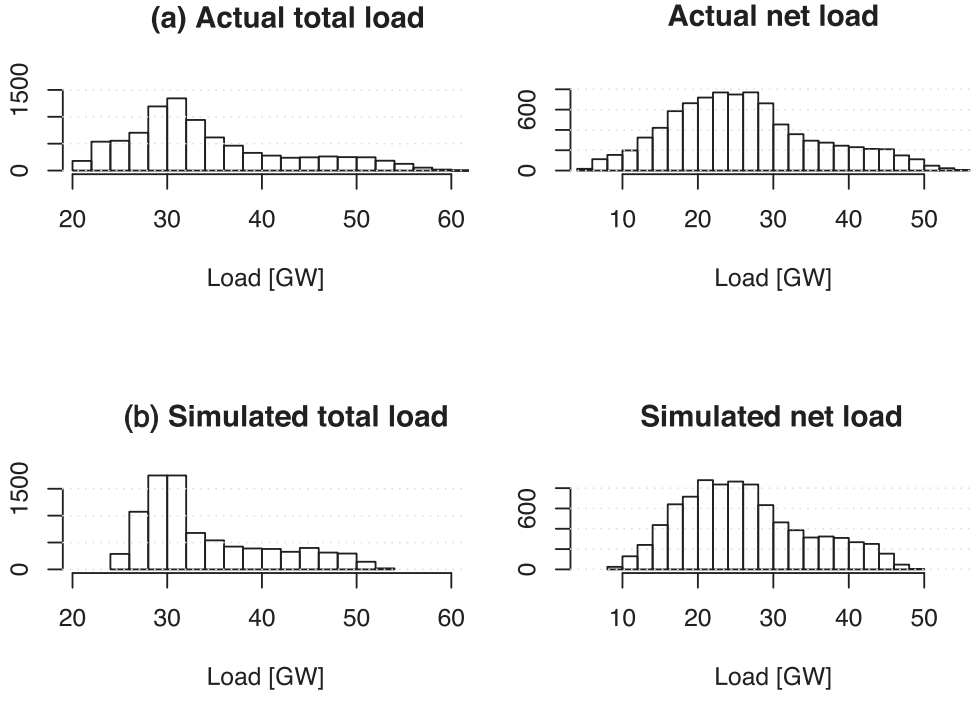

Figure 11. Histograms comparing 2005 actual and simulated base case total and net load.

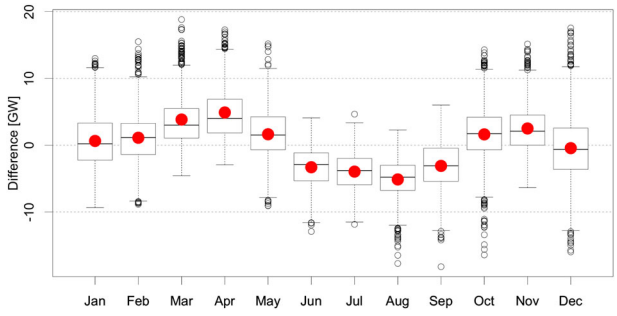

Figure 12. Hourly residual errors between simulated and actual ERCOT load by month. Note that the load is overpredicted in the spring and fall seasons and underpredicted in the summer. The mean and median of residual errors are least in the winter.

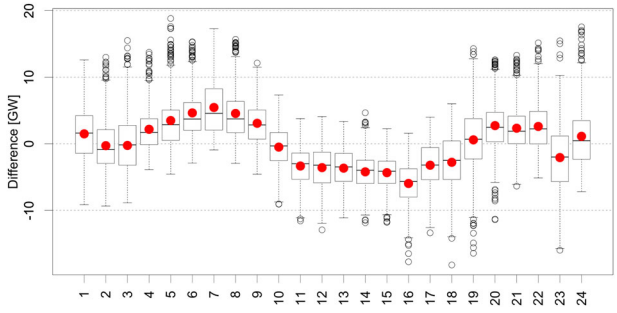

Figure 13. Residual errors between simulated and actual ERCOT load by the hour of day. Note that the load is overpredicted in the morning before and after sunrise, underpredicted in the middle of the day, and overpredicted in the evening. The mean and median of residual errors are least in hours 2, 3, 10, 19, and 24.

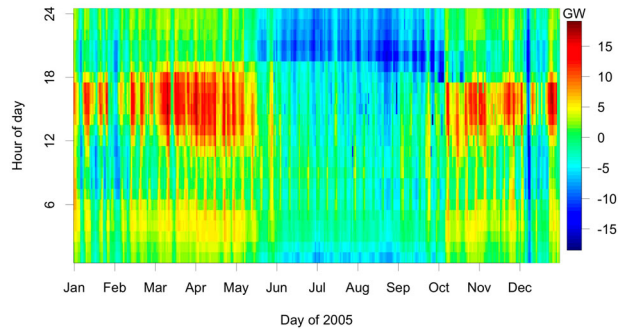

Figure 14. Heat map of errors between simulated and actual ERCOT load. Note the spring and fall versus summer season behaviour. Weak seasonal stationarity of residuals is apparent among adjacent days as denoted by similar colour signatures.

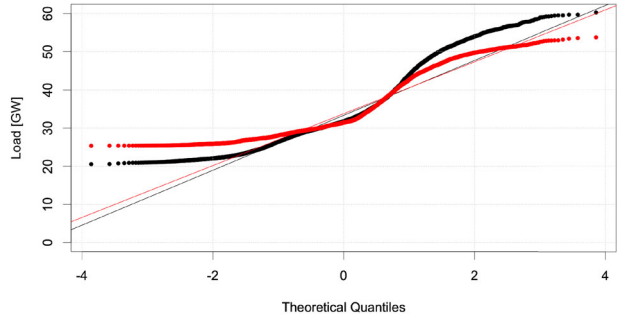

Figure 15. Overlaid quantile-quantile plots of simulated versus actual ERCOT load. The black dots depict actual load, and the red dots depict simulated load.

which has a reduced range of loads. The left of Figure 11 depicts the total load and the right shows the simulated net load after subtracting the actual time-synchronous RES.

To quantify whether the model was systematically underpredicting or overpredicting the simulated load, the mean bias error was calculated for the year by subtracting the hourly actual load from the predicted load, and was found to be zero. Monthly box plot distributions were created to compare the hourly errors between simulated and actual load, as shown in Figure 12.

Figure 12 indicates the best agreement between simulated and actual load during the winter, over prediction during the spring and fall, and underprediction during the summer.

To provide additional insight into the distribution of residual errors, box plot distributions were created to compare the hourly errors between simulated and actual load by the hour of day, as shown in Figure 13.

To visualize the information in Figures 12 and 13, a heat map was used to depict residual errors by hour for each day over the course of a year, as shown in Figure 14.

Figure 14 depicts (1) the greatest over predictions occurred in the winter, spring, and fall seasons in the late afternoon and early evening, and (2) the greatest underpredictions occurred in the summer in the late evening. Referencing Figure 10(a,b), the summer evening *simulated* load decreased faster than *actual* load starting at hour 20.

To further investigate the performance of the model, the quantiles of simulated versus actual values were plotted against each other, as shown in Figure 15.

In Figure 15 the black dots depict actual load. The red dots depict simulated load, which is overpredicted at low loads and underpredicted at high loads. Per Figures 11–15, there is evidence to reject the assumption that the electric load data are normally distributed.

To simplify the interpretation of Figure 15, the quantiles of simulated versus historical values were plotted against each other, as shown in Figure 16.

Lastly, a two-sample Kolmogorov-Smirnov Test was used to compare the simulated and actual load for the year. The test is a nonparametric distribution-independent evaluation comparing the simulated and

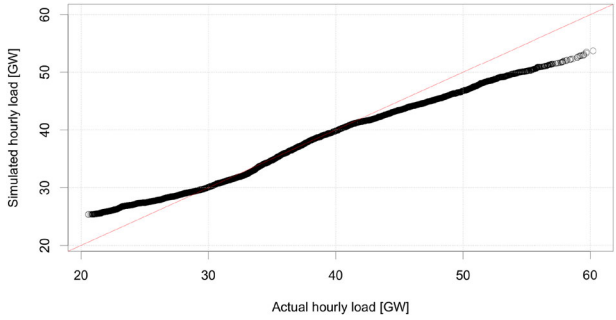

Figure 16. Quantile-quantile plot of simulated versus actual ERCOT load. The residual errors of the model are depicted by the distance from the diagonal. This visualization also indicates that simulated load is overpredicted at low loads and underpredicted at high loads.

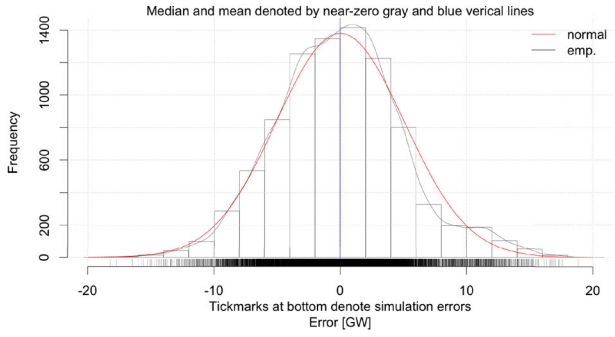

Figure 17. Histogram of errors between actual and simulated ERCOT load. An empirical distribution and normal distribution are overlaid for reference.

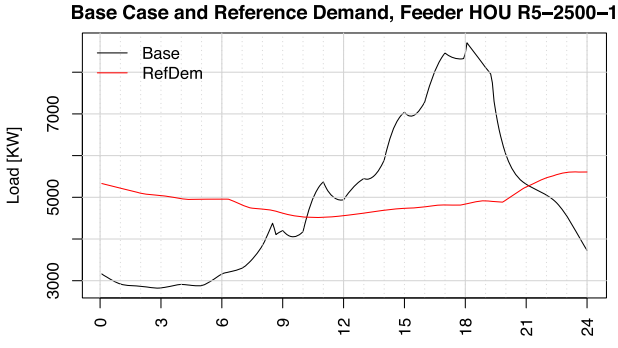

Figure 18. Base Case and reference demand for 2146 homes on Houston Feeder R5-2500-1 on 20 Jul 2005.

actual samples and is sensitive to differences in both location and shape of the empirical cumulative distribution functions of the two samples. Given a significance level of 0.05, the near-zero *p*-value of 2.2e−16 provides evidence to reject the null hypothesis that the two samples were drawn from the same distribution.

A histogram of the residual errors are shown in Figure 17.

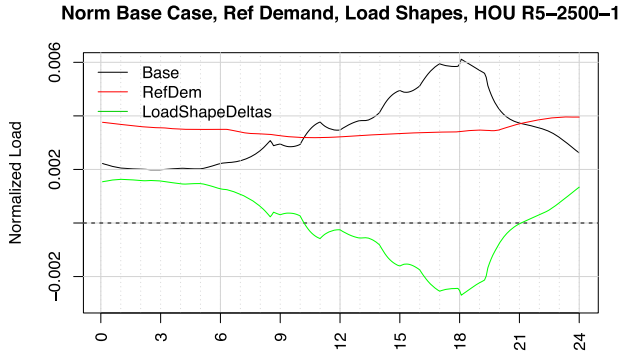

Figure 19. Normalized Base Case, reference demand, and load shape deltas for Houston Feeder R5-2500-1 on 20 July 2005.

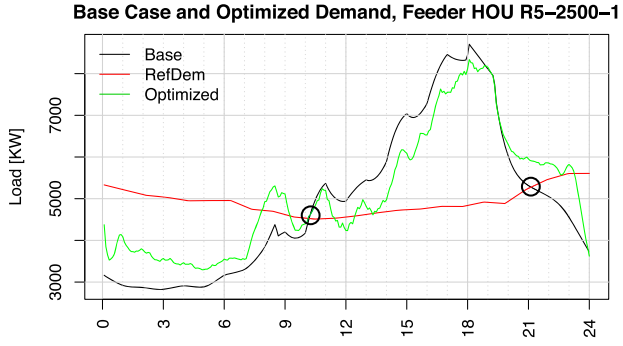

Figure 20. Base Case, reference demand, and MPC optimized air conditioning demand for Houston Feeder R5-2500-1 on 20 July 2005.

In Figure 17, the residual errors of the simulated less the actual loads are nearly normally distributed.

Referencing Figures 11 and 14–17, the model overpredicted low loads less than it underpredicted high loads. The impact of underpredicting high loads is critically important as it introduces errors that significantly impact the power systems planning process. First, it underestimates the amount of required peak generation capacity, which is most often the most expensive capacity per unit of electricity produced. Second, it underestimates the marginal cost of generation during high-load and peak demand periods. Failing to predict the highest loads results in failing to simulate the operation of the most expensive marginal generation, which results in significantly underestimating the cost of high-load and peak demand periods.

4.5. MPC load shaping

For Cases 9–15, MPC-enabled load shaping was simulated on individual devices, with resulting loads, including generic loads, aggregated at the house level. Depending on feeder size, between 168 and 2192 homes were aggregated to reflect the load at the feeder level. Device loads,

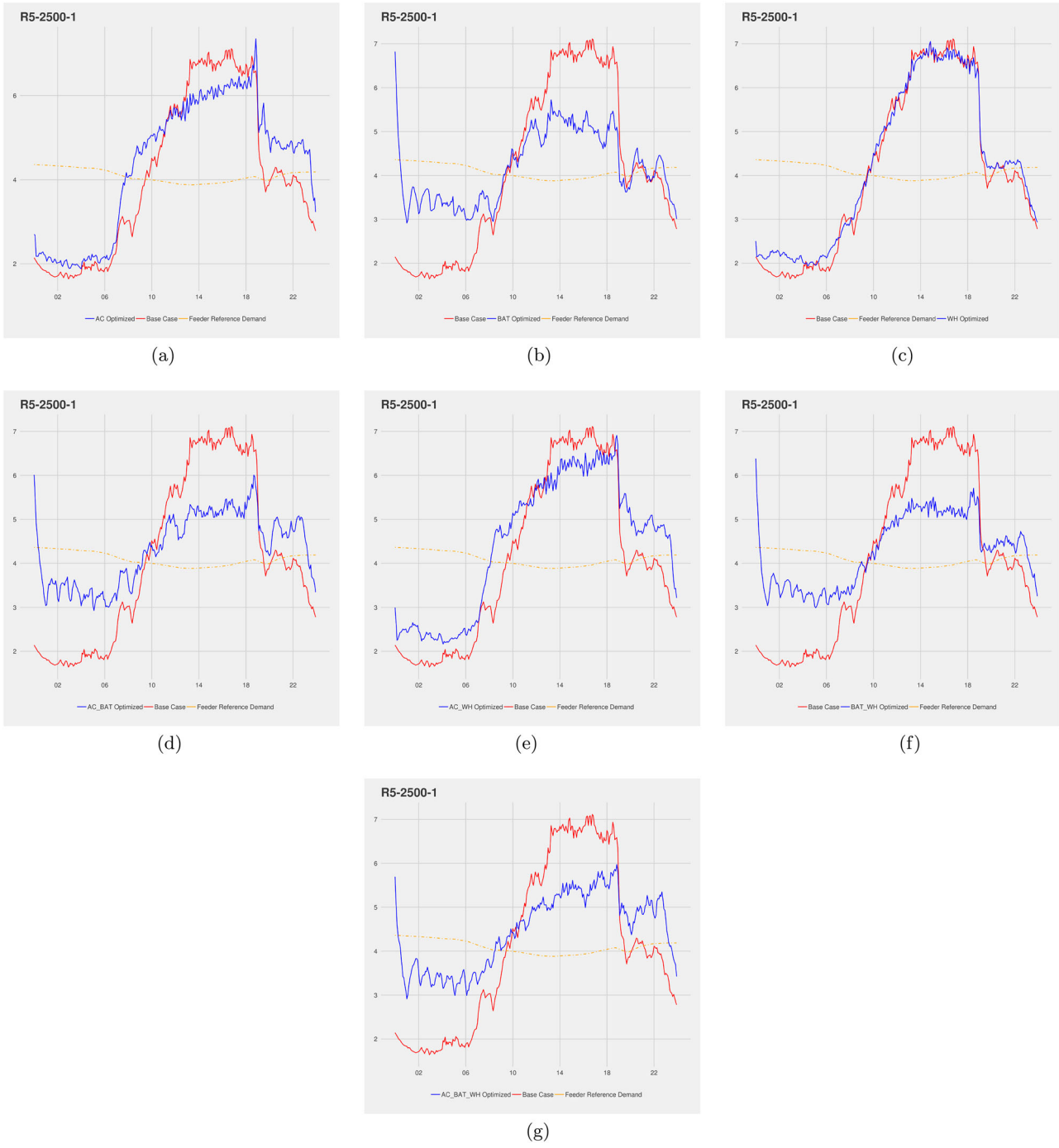

Figure 21. Scenario A load shapes for Houston Feeder R5-2500-1, 18 May 2005. GridMPC attempted to increase the Optimized load above the Base Case load until hour 9:30, decrease from hours 9:30–19:30, and increase from hours 19:30–24:00. While the response in each of (a)–(g) is unique, similar load add and shed trends were apparent. (a) Air Conditioning. (b) Battery. (c) Water heater. (d) Air Conditioning + Battery. (e) Air Conditioning + Water heater. (f) Battery + Water heater and (g) Air Conditioning + Battery + Water heater.

generic house loads, and feeder loads were recorded for verification of intended behaviour and further post-processing. For example, the Base Case simulated load and the Reference Demand (scaled from the daily OLS) for Houston Feeder R5-2500-1 are shown in Figure 18.

In Figure 18, the Reference Demand (in red) informs GridMPC to add load when above the Base load (in black) until hour 10, to shed load when below the Base load between hours 10 and 21, and then to add load again starting in hour 21 through the end of the day.

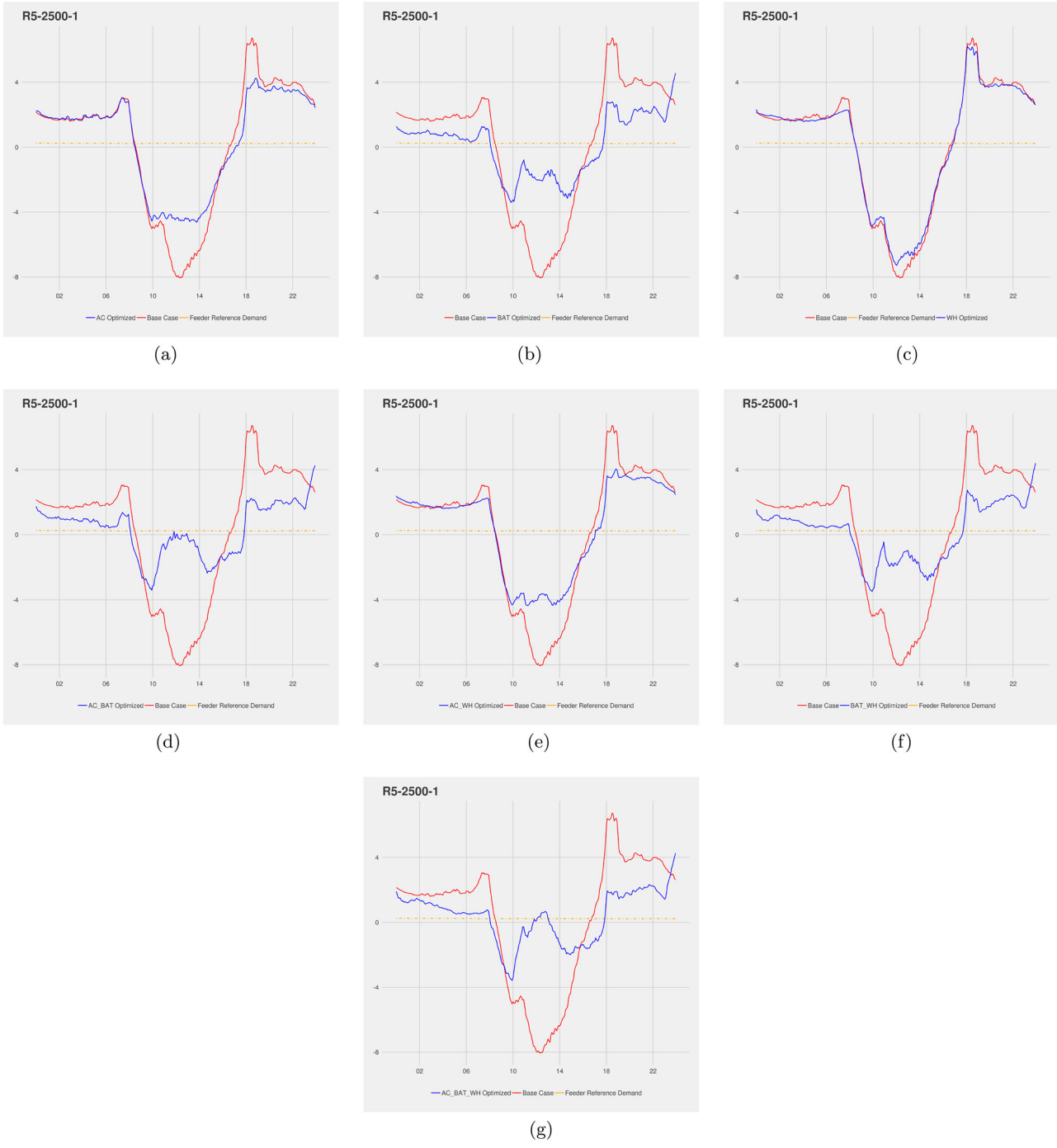

Figure 22. Scenario B load shapes for Houston Feeder R5-2500-1, 18 May 2005. The Feeder Reference Demand was nearly flat. Fifty percent of homes having net-zero PV resulted in mid-day negative generation denoted by the red dip. As expected, GridMPC added load to offset PV generation. Differing performance of load shaping were apparent in (a)–(g). (a) Air Conditioning. (b) Battery. (c) Water heater. (d) Air Conditioning + Battery. (e) Air Conditioning + Water heater. (f) Battery + Water heater and (g) Air Conditioning + Battery + Water heater.

Continuing the example, using the method of Corbin and Henze, feeder loads and Reference Demand were normalized and then differenced to produce the daily OLS deltas shown in Figure 19.

In Figure 19, the green line connects the 288, five-minute load shape deltas, creating a zero-centered inverse of the normalized load less the reference demand.

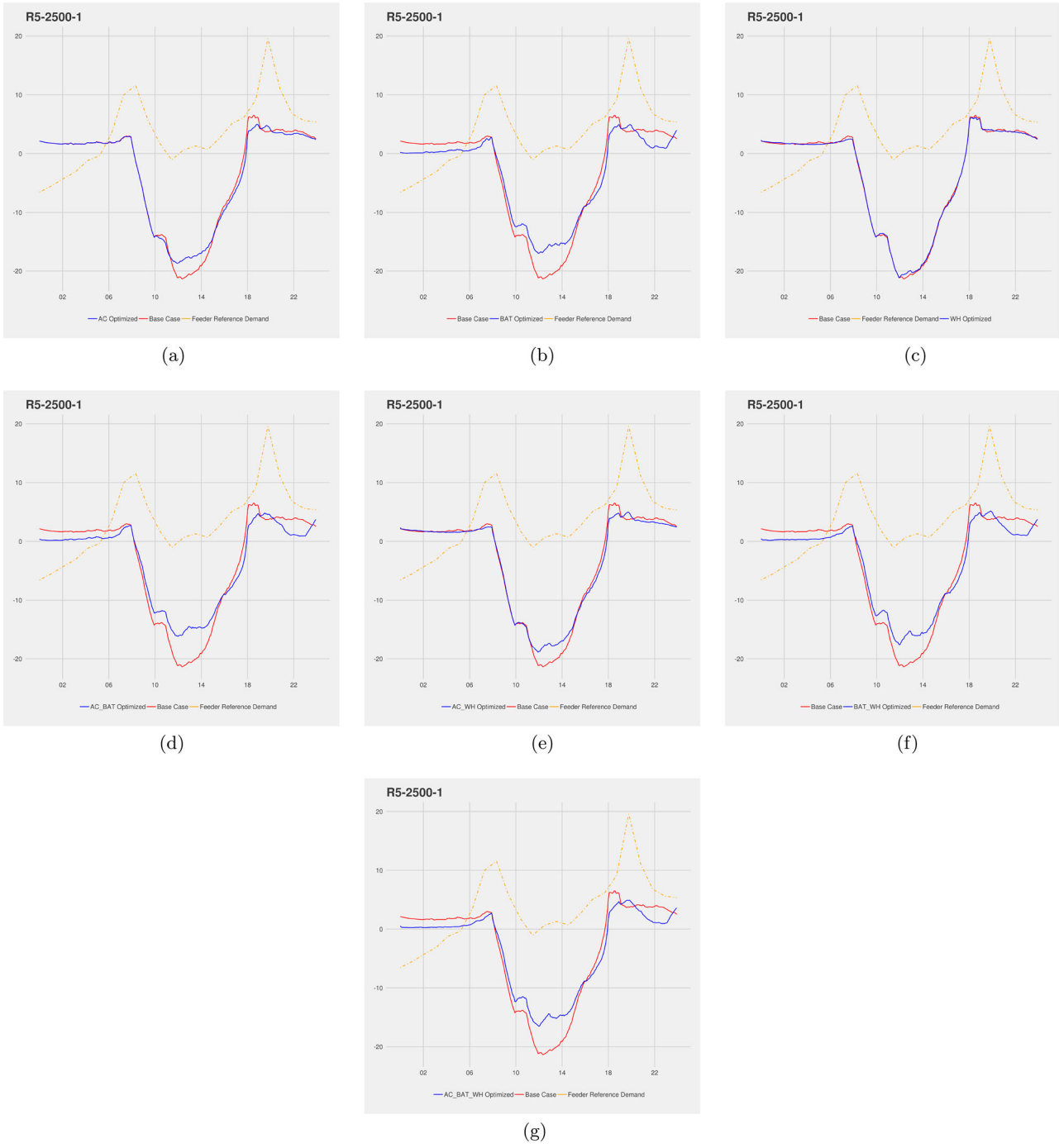

Figure 23. Scenario C load shapes for Houston Feeder R5-2500-1, 18 May 2005. The Feeder Reference Demand specified shedding load until hour 6 and adding load thereafter. All homes having net-zero PV resulted in greater mid-day negative generation denoted in red. GridMPC added load but was unable to completely offset PV generation. (a) Air Conditioning. (b) Battery. (c) Water heater. (d) Air Conditioning + Battery. (e) Air Conditioning + Water heater. (f) Battery + Water heater and (g) Air Conditioning + Battery + Water heater.

For Case 9, simulated shaped load with MPC of air conditioning (A/C), applying the daily OLS deltas resulted in the optimized load shown in Figure 20. The calculations for Cases 10–15 followed the same process.

In Figure 20, the circle at hour 10 denotes MPC transition from load adding in the morning to load shedding in the middle of the day. Likewise, the circle at hour 21 denotes MPC transition from load shedding in the middle of the day to load adding at night. In this example, there are two transitions denoted by circles, though the simulation supports up to 288 transitions per day given 5-minute intervals. The specific timing and number of

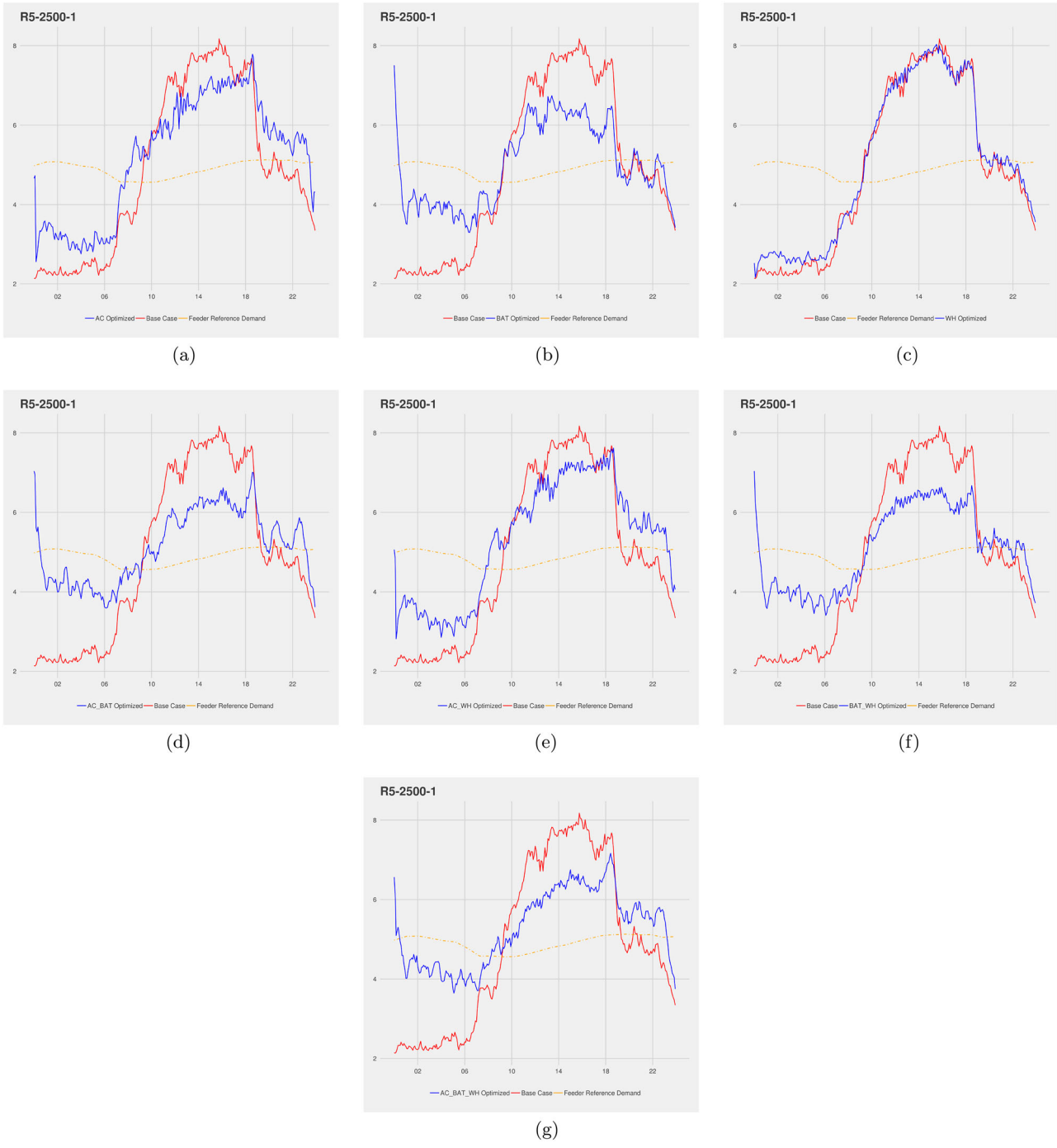

Figure 24. Scenario A load shapes for Houston Feeder R5-2500-1, 23 Aug 2005. Load shaping benefits occurred (a) in hours 1–22, and 6, (b) in hours 1–18, and (c) in hours 1–7, 19, and 21. Although not an exact superposition of benefits, complementary load shaping occurred across managed loads, for example, in hours 1–6 where the benefit in (e) is greater than in (a) and (c). (a) Air Conditioning. (b) Battery. (c) Water heater. (d) Air Conditioning + Battery. (e) Air Conditioning + Water heater. (f) Battery + Water heater and (g) Air Conditioning + Battery + Water heater.

transitions per day varied depending on the simulated Base Case load and the OLS. In theory, given sufficient computational resources, there is no upper limit on the number of transitions possible. To simplify interpretation, the load curves in Figures 18–20 were kept as smooth as possible by simulating the air conditioning portion of the load (for these figures only) with infinitely variable home air conditioners that had no minimum on-time requirement.

On some days, the impacts of ARLS were negligible, slightly positive or negative, such as (1) in Scenario A, when RES was fully utilized regardless of the application

Figure 25. Scenario B load shapes for Houston Feeder R5-2500-1, 23 Aug 2005. load shaping benefits occurred (a) in hours 6–22, and 6, (b) in hours 3–22, and (c) in hours 7 and 13. Complementary load shaping occurred across managed loads in (d) in hours 4–22, (e) in hour 7, (f) hours 3–8 and 19–21, and (g) which had the smoothest optimized load. (a) Air Conditioning. (b) Battery. (c) Water heater. (d) Air Conditioning + Battery. (e) Air Conditioning + Water heater. (f) Battery + Water heater and (g) Air Conditioning + Battery + Water heater.

of the OLS, and (2) in Scenarios B and C, when there was sufficient hourly RES throughout the day such that thermal generation was unneeded. On other days, the impacts of ARLS were considerable and are detailed here.

The 18th of May 2005 and the 23rd of August 2005 were further examined for analysis of MPC-based control based on ARLS. The performance of ARLS on 18 May 2005 and 23 Aug 2005 is shown for Cases 9–15, Scenarios A, B, and C in Figures 21–26. The objective of GridMPC in all Cases and Scenarios was to shape and modulate load to match – as closely as possible – the Feeder Reference Demand. The Feeder Reference

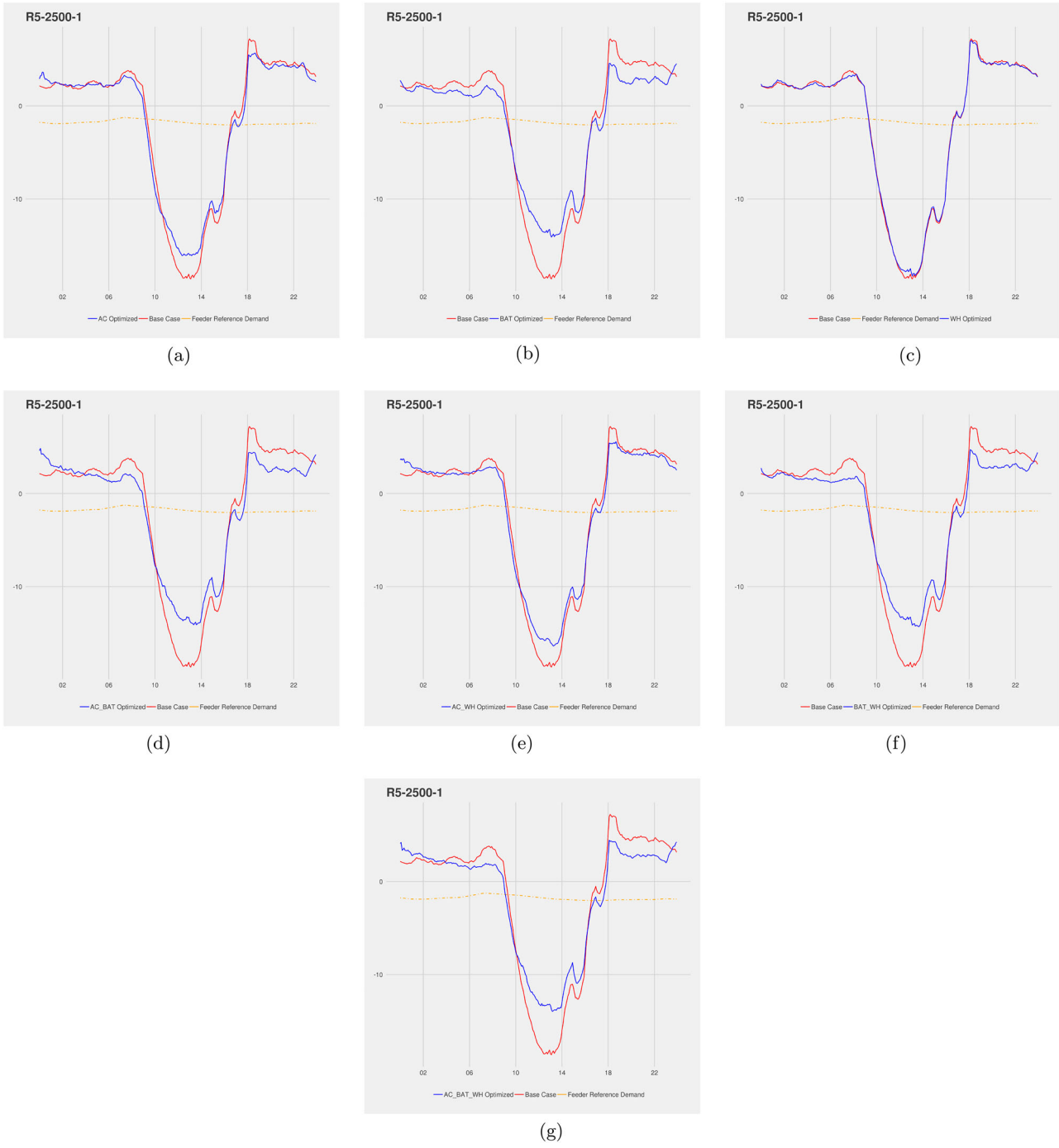

Figure 26. Scenario C load shapes for Houston Feeder R5-2500-1, 23 Aug 2005. Load shaping benefits occurred (a) in hours 11–13, and 6, (b) in hours 1–22, and (c) in hours 7 and 12. Complementary load shaping occurred across managed loads in (e) hour 7, (f) hour 8, and (g) with the smoothest optimized load. Undesired load add occurred in (d), (e), and (g) in hours 1–3. (a) Air Conditioning. (b) Battery. (c) Water heater. (d) Air Conditioning + Battery. (e) Air Conditioning + Water heater. (f) Battery + Water heater and (g) Air Conditioning + Battery + Water heater.

Demand was the OLS adjusted to account for local generation on the feeder from residential PV. This was accomplished by GridMPC minimizing the differences between the Optimized demand and Feeder Reference Demand.

In Figures 21–26, the Feeder Reference Demand, depicted by the gold dot-dash line, was calculated by scaling down the ERCOT daily optimal load shape such that daily energy use (i.e. the area under the curve) was the same as the Base Case energy use depicted in red.

In every MPC Case and RES penetration scenario, the Feeder Reference Demand was the control signal used by GridMPC to add or shed load throughout the day.

In Figures 21–26, large excursions in the air-conditioning optimized loads at the start of each day denote initial cool down of homes. Large excursions in the battery optimized load at the start of each day denote a rapid change from the initial SOC of 50% and highlight the ability of batteries to immediately and rapidly charge or discharge as directed by GridMPC in response to the Feeder Reference Demand. In addition, large excursions in the battery optimized load at the end of each day denote GridMPC attempting to return the battery to a final SOC of 50%. These edge effects could be mitigated with a multi-day model, which would likely predict greater savings through more seamless orchestration of air-conditioning- and battery-enabled storage across days.

Figures 21–23 provide insight to the behaviour of ARLS on a spring day as annotated in the text following each figure. Figures 24–26 detail the behaviour of ARLS on a peak load day occurring in summer. Higher loads that are driven by air-conditioning are apparent. As hypothesized in Section 3.2.2, the MPC of DERs can be complementary in supporting the grid at different times of the day, as explained in the text following Figures 21–26.

An important takeaway from Figures 21–26 is that residential load can be shaped significantly in order to take advantage of increasing penetrations of RES. From a practical perspective and for the purposes of this study, the loads that were shaped were those with inherent thermal or electrical storage. Excluded from the analysis were loads from lighting and miscellaneous electric loads such as plug loads.

5. Conclusions

This calibrated simulation study created a broad geographic assessment of the impact of residential load flexibility on variable production costs and CO_2 emissions that can be useful for decision and policymakers. Unique to this study was the combination of physical load and generation models to estimate the impact of residential load flexibility on the generation of electric power for the state of Texas. The methodology estimated the monetary savings that electricity producers could realize by jointly optimizing residential energy use and the mix of generation under scenarios of increasing penetrations of renewable energy – with savings as an essential metric in deciding whether OLS and ARLS are worthy of further research and implementation (Electric Reliability Council of Texas 2019a). The methodology is suitable for use in small and large grids (i.e. nanogrids, microgrids, and macrogrids) in other world geographies, requiring only knowledge of historical load, weather, attributes of the building stock, operating schedules of electrical devices, distribution feeder models, generator constraints, and fuel costs.

Throughout its 139 year history, electric power production has typically been optimized only to meet the anticipated inflexible load and required reserves at the lowest possible cost (Soroudi 2017). By including flexible residential load as an additional dimension of optimization, ARLS introduced a new paradigm in the traditional supply-follows-demand relationship by managing storage-capable loads to shift forward or backward in time in order to follow and use the least costly forms of generation. The effect of time-shifting residential demand at high penetrations of RES was twofold: (a) it reduced electric power production costs by shaping load to increase the efficiency of thermal generation, and (b) it decreased the curtailment of RES by encouraging demand to follow the least costly forms of supply – while providing for user needs and maintaining user comfort.

With the ability of ARLS to move load away from more costly generators towards less costly generators, the opportunity for reduction in production costs increased as a function of RES penetration. The maximum opportunity for savings at the highest penetrations of RES was a 1/3 reduction in annual production costs, from $3.2B to $1.9B, and a 1/5 reduction in annual CO_2 emissions, from 95B to 78B tons.

Modelling enormous changes in load and RES can result in a seachange in the operation of thermal generation – and gross errors in electricity production costs. To wit, in the presence of highly penetrated RES, as fossil-fuelled base load, mid-merit, and peaking generators run less often, their marginal production cost will increase, likely skewing cost calculations in favour of ARLS as thermal generation becomes less competitive.

Disclosure statement

No potential conflict of interest was reported by the author(s).

Funding

This work was authored in part by the National Renewable Energy Laboratory, operated by Alliance for Sustainable Energy, LLC, for the U.S. Department of Energy (DOE) under Contract No. DE-AC36-08GO28308. Funding provided by U.S. Department of Energy Office of Energy Efficiency and Renewable Energy. The views expressed in the article do not necessarily represent the views of the DOE or the U.S. Government. The U.S. Government retains and the publisher, by accepting the article for publication, acknowledges that the U.S. Government retains a nonexclusive, paid-up, irrevocable, worldwide license to publish or reproduce the published form of this work, or allow others to do so, for U.S. Government purposes.

ORCID

Robert Cruickshank http://orcid.org/0000-0001-7268-9132
Gregor Henze http://orcid.org/0000-0002-4084-9709
Anthony Florita http://orcid.org/0000-0002-8998-6106
Charles Corbin http://orcid.org/0000-0003-1639-1555

References

American National Standards Institute/Society of Cable Tele communications Engineers. 2021. "ANSI/SCTE 267 2021 Optimum Load Shaping for Electric Vehicle and Battery Charging." Accessed 7 July 2021. https://www.scte.org/standards-development/library/standards-catalog/optimum-load-shaping-for-electric-vehicle-and-battery-charging.

Anisie, A. 2019. *Innovation Landscape for a Renewable-Powered Future*. International Renewable Energy Agency, Latham, NY, USA.

Barley, C. D., and C. B Winn. 1996. "Optimal Dispatch Strategy in Remote Hybrid Power Systems." *Solar Energy* 58 (4-6): 165–179. doi:10.1016/S0038-092X(96)00087-4.

Barley, C. D., C. B. Winn, L. Flowers, and H. Green. 1995. "Optimal Control of Remote Hybrid Power Systems, Part 1: Simplified Model." In *Proceedings Windpower '95*, Washington, DC, USA, 1–11.

Battelle Memorial Institute. 2017. "GridLAB-D: Residential/Water heater.Cpp Source File." Accessed 17 July 2019. https://github.com/gridlab-d/gridlab-d/blob/master/residential/waterheater.cpp.

Bessa, R., C. Moreira, B. Silva, and M. Matos. 2019. "Handling Renewable Energy Variability and Uncertainty in Power System Operation." In *Advances in Energy Systems*, 1–26. Wiley. doi:10.1002/9781119508311.ch1.

Brandemuehl, M. J. 1993. *HVAC 2 Toolkit: A Toolkit for Secondary HVAC System Energy Calculations, American Society of Heating, Refrigerating and Air-Conditioning Engineers*.

Burch, J. 2012. "A Realistic Hot Water Draw Specification for Rating Solar Water Heaters." In *Proceedings World Renewable Energy Forum Denver*, Denver, Colorado, USA, 1–8.

Chassin, D. P., J. C. Fuller, and N. Djilali. 2014. "GridLAB-D: An Agent-Based Simulation Framework for Smart Grids." *Journal of Applied Mathematics* 2014: 1–12. doi:10.1155/2014/492320.

Corbin, C. D., and G. Henze. 2017a. "Predictive Control of Residential HVAC and Its Impact on the Grid. Part I: Simulation Framework and Models." *Journal of Building Performance Simulation* 10 (3): 294–312. doi:10.1080/19401493.2016.1231220.

Corbin, C. D., and G. Henze. 2017b. "Predictive Control of Residential HVAC and Its Impact on the Grid. Part II: Simulation Studies of Residential HVAC As a Supply Following Resource." *Journal of Building Performance Simulation* 10 (4): 365–377. doi:10.1080/19401493.2016.1231221.

Corbin, C. D. July 2014. "Assessing Impact of Large Scale Distributed Residential HVAC Control Optimization and Electricity Grid Operation and Renewable Energy Integration." Ph.D. thesis, Boulder, CO: University of Colorado Boulder.

Craig, M. T., M. Rossol, B.-M. Hodge, C. Brancucci, and I. L. Carreno. 2019. "Effects on Power System Operations of Potential Changes in Wind and Solar Generation Potential Under Climate Change." *Environmental Research Letters* 14 (3): Article ID 034014. doi:10.1088/1748-9326/aaf93b.

Cruickshank, R. F., A. R. Florita, G. P. Henze, and C. D. Corbin. 2018. "Characterizing Electric Grid System Benefits of MPC-Based Residential Load Shaping." In *Proceedings of 2018 Building Performance Analysis Conference and SimBuild, co-organized by ASHRAE and IBPSA-USA*, 791–798. Chicago, IL.

Cruickshank, R. F., G. P. Henze, R. Balaji, B.-M. S. Hodge, and A. R. Florita. 2017. "Empirical Investigations of the Opportunity Limits of Automatic Residential Electric Load Shaping." In *Proceedings of the IEEE 9th Annual Green Technologies Conference*, 75–82. Denver, CO. doi:10.1109/greentech.2017.17.

Deetjen, T. A., J. D. Rhodes, and M. E. Webber. 2017. "The Impacts of Wind and Solar on Grid Flexibility Requirements in the Electric Reliability Council of Texas." *Energy* 123: 637–654. doi:10.1016/j.energy.2017.02.021.

Eissa, M., S. Wasfy, and M. Sallam. 2012. "Load Management System Using Intelligent Monitoring and Control System for Commercial and Industrial Sectors." In *Energy Efficiency*, edited by M. Eissa, 3–18. Rijeka: IntechOpen. Ch. 1. doi:10.5772/51850.

Electric Reliability Council of Texas. 2005. "ERCOT Hourly Load Data Archives." Accessed 8 June 2019. http://www.ercot.com/gridinfo/load/load_hist.

Electric Reliability Council of Texas. 2019a. "About ERCOT." Accessed 8 June 2019. http://www.ercot.com/about.

Electric Reliability Council of Texas. 2019b. "ERCOT Weather Zone Map." Accessed 18 July 2019. http://www.ercot.com/news/mediakit/maps.

Energyplus. 2018. "Engineering Reference." Accessed 3 August 2019. https://energyplus.net/sites/all/modules/custom/nrel_custom/pdfs/pdfs_v8.9.0/EngineeringReference.pdf.

EPA. 2020. "Inventory of U.S. Greenhouse Gas Emissions and Sinks: 1990–2018." Accessed 19 May 2020. https://www.epa.gov/ghgemissions/sources-greenhouse-gas-emissions.

Evans, P., and M. Annunziata. 2012. "Industrial Internet: Pushing the Boundaries of Minds and Machines." General Electric.

General Electric. 2019. "Global Power Plant Efficiency Analysis." Accessed 8 June 2019. https://www.ge.com/reports/wp-content/themes/ge-reports/ge-power-plant/dist/pdf/GE%20Global%20Power%20Plant%20Efficiency%20Analysis.pdf.

Helistö, N., J. Kiviluoma, J. Ikäheimo, T. Rasku, E. Rinne, C. O'Dwyer, R. Li, and D. Flynn. 2019. "Backbone–an Adaptable Energy Systems Modelling Framework." *Energies* 12 (17): 3388. doi:10.3390/en12173388.

Hendron, B., J. Burch, and B. G. Journal. 2010. "Tool for Generating Realistic Residential Hot Water Event Schedules." *IBPSA-USA Journal*.

Hendron, R., and C. Engebrecht. 2010. *Building America House Simulation Protocols (Revised)*. Tech. Rep. TP-550-49426, National Renewable Energy Laboratory.

Hungerford, Z., A. Bruce, and I. MacGill. 2019. "The Value of Flexible Load in Power Systems with High Renewable Energy Penetration." *Energy* 188: Article ID 115960. doi:10.1016/j.energy.2019.115960.

International Civil Aviation Organization. 2019. "Location Identifiers." Accessed 5 August 2018. https://cfapp.icao.int/MET/MET_7910Ref.aspx.

International Energy Agency. 2019. "Key World Energy Statistics 2018." Accessed 8 June 2019. https://webstore.iea.org/download/direct/2291?fileName = Key_World_2018.pdf.

I. Tesla. 2019. "Powerwall." Accessed 19 July 2019. https://www.tesla.com/powerwall.

Jin, X., K. A. Baker, D. T. Christensen, and S. Isley. 2017. "Foresee: A User-centric Home Energy Management System for Energy Efficiency and Demand Response." *Applied Energy* 205: 1583–1595. doi:10.1016/j.apenergy.2017.08.166.

Kaabeche, A., and R. Ibtiouen. 2014. "Techno-economic Optimization of Hybrid Photovoltaic/wind/diesel/battery Generation in a Stand-alone Power System." *Energy Procedia* 103: 6384–6392. doi:10.1016/j.solener.2014.02.017.

Kaufman, N., and K. Gordon. 2018. *The Energy, Economic, and Emissions Impacts of a Federal U.S. Carbon Tax*. Tech. Rep., Columbia University, SIPA Center on Global Energy Policy. https://energypolicy.columbia.edu/research/report/energy-economic-and-emissions-impacts-federal-us-carbontax.

Kessels, K., C. Kraan, L. Karg, S. Maggiore, P. Valkering, and E. Laes. 2016. "Fostering Residential Demand Response Through Dynamic Pricing Schemes: A Behavioural Review of Smart Grid Pilots in Europe." *Sustainability* 8 (9): 929. doi:10.3390/su8090929.

Kondoh, J., N. Lu, and D. J. Hammerstrom. 2011. "An Evaluation of the Water Heater Load Potential for Providing Regulation Service." *IEEE Transactions on Power Systems* 26 (3): 1309–1316.

Larson, B., L. Gilman, R. Davis, M. Logsdon, J. Uslan, B. Hannas, D. Baylon, P. Storm, V. Mugford, and N. Kvaltine. 2014. "Residential Building Stock Assessment: Metering Study." Northwest Energy Efficiency Alliance. Accessed 7 June 2019. https://neea.org/img/documents/residential-building-stock-assessment-metering-study.pdf.

Lee, U., J. Han, A. Elgowainy, and M. Wang. 2018. "Regional Water Consumption for Hydro and Thermal Electricity Generation in the United States." *Applied Energy* 210: 661–672. doi:10.1016/j.apenergy.2017.05.025.

Li, S., W. Zhang, J. Lian, and K. Kalsi. 2016a. "Market-based Coordination of Thermostatically Controlled Loads–Part I: A Mechanism Design Formulation." *IEEE Transactions on Power Systems* 31 (2): 1170–1178. Team-Optimal DLC Solution for thermostats,

Li, S., W. Zhang, J. Lian, and K. Kalsi. 2016b. "Market-Based Coordination of Thermostatically Controlled Loads–Part II: Unknown Parameters and Case Studies." *IEEE Transactions on Power Systems* 31 (2): 1179–1187. From Chad Corbin. doi:10.1109/TPWRS.2015.2432060.

Liu, Z., I. Liu, S. Low, and A. Wierman. 2014a. "Pricing Data Center Demand Response." *ACM SIGMETRICS Performance Evaluation Review* 42 (1): 111–123. doi:10.1145/2637364.2592004.

Liu, Z., I. Liu, S. Low, and A. Wierman. 2014b. "Pricing Data Center Demand Response." In *Proceedings SIGMETRICS '14*, Austin, Texas, USA 111–123.

Lovins, A. B. 2013. *Reinventing Fire: Bold Business Solutions for the New Energy Era*. Old Snowmass, Colorado: Rocky Mountain Institute.

Ma, Z., H. T. A. Friis, C. G. Mostrup, and B. N. Jørgensen. 2017. "Energy Flexibility Potential of Industrial Processes in the Regulating Power Market." In *Proceedings of the 6th International Conference on Smart Cities and Green ICT Systems*, 109–115. doi:10.5220/0006380201090115.

Mikkola, J., and P. D. Lund. 2016. "Modeling Flexibility and Optimal Use of Existing Power Plants with Large-Scale Variable Renewable Power Schemes." *Energy* 112: 364–375.

Miller, N. W., M. Shao, S. Pajic, and R. D'Aquila. December 2014. *Western Wind and Solar Integration Study Phase 3 – Frequency Response and Transient Stability*. Tech. Rep. NREL/SR-5D00-62906, National Renewable Energy Laboratory and GE Energy Management. doi:10.2172/1167065.

Montenegro, D., and R. C. Dugan. 2017. OpenDSS and OpenDSS-PM Open Source Libraries for NI LabVIEW." In *2017 IEEE Workshop on Power Electronics and Power Quality Applications (PEPQA)*, 1–5. doi:10.1109/pepqa.2017.7981639.

National Oceanic and Atmospheric Administration. 2019. "Integrated Surface Database." Accessed 5 August 2018. https://www.ncdc.noaa.gov/isd.

Newsham, G. R., and B. G. Bowker. 2010. "The Effect of Utility Time-varying Pricing and Load Control Strategies on Residential Summer Peak Electricity Use: A Review." *Energy Policy* 38 (7): 3289–3296. doi:10.1016/j.enpol.2010.01.027.

N. RBSA. 2017. "Regional Data Resources and Building Stock Assessments."

NRDC. 2020. "The Myth of the 24/7/365 Power Plant." Accessed 19 May 2020. https://www.nrdc.org/experts/rachel-fakhry/myth-247365-power-plant.

Pacific Northwest National Laboratory. 2018. "GridLAB-D Matlab Feeder Generation Scripts." Accessed 5 August 2018. https://github.com/gridlab-d/Taxonomy_Feeders/tree/master/PopulationScript.

Peer, R. A., and K. T. Sanders. 2018. "The Water Consequences of a Transitioning US Power Sector." *Applied Energy* 210: 613–622. doi:10.1016/j.apenergy.2017.08.021.

Pratt, A., D. Krishnamurthy, M. Ruth, H. Wu, M. Lunacek, and P. Vaynshenk. 2016. "Transactive Home Energy Management Systems: The Impact of Their Proliferation on the Electric Grid." *IEEE Electrification Magazine* 4: 8–14.

Ren21. 2019. "Renewables 2018 Global Status Report." Accessed 8 June 2019. http://www.ren21.net/gsr-2018/.

Schneider, K. P. November 2008. *Modern Grid Initiative: Distribution Taxonomy Final Report*. Tech. Rep. PNNL-18035, Pacific Northwest National Laboratory.

Shaker, H., D. Manfre, and H. Zareipour. 2020. "Forecasting the Aggregated Output of a Large Fleet of Small Behind-the-meter Solar Photovoltaic Sites." *Renewable Energy* 147: 1861–1869. doi:10.1016/j.renene.2019.09.102.

Sklar, S. 1990. "The Role of the Federal Government in the Commercialization of Renewable Energy Technologies." *Annual Review of Energy* 15: 121–132. doi:10.1146/annurev.eg.15.110190.001005.

Soroudi, A. 2017. *Power System Optimization Modeling in GAMS*. Belfield, Leinster: Springer.

U. DOE. 2017a. "GridLAB-D: Residential/Freezer.CPP Source File."

U. DOE. 2017b. "GridLAB-D: Residential/Refrigerator.CPP Source File."

U.S. Energy Information Administration. 2009. "Residential Energy Consumption Survey (RECS): 2009 Survey Data." https://www.eia.gov/consumption/residential/data/2009/.

Zhang, J., A. Florita, B.-M. Hodge, S. Lu, H. F. Hamann, V. Banunarayanan, and A. M. Brockway. 2015. "A Suite of Metrics for Assessing the Performance of Solar Power Forecasting." *Solar Energy* 111: 157–175. doi:10.1016/j.solener.2014.10.016.